1.0

2.8   2.5

3.2   2.2

3.0

2.0

1.1

1.8

1.25   1.4   1.6

MICROCOPY RESOLUTION TEST CHART

NATIONAL BUREAU OF STANDARDS

DAVID W. TAYLOR NAVAL SHIP
RESEARCH AND DEVELOPMENT CENTER

Bethesda, Maryland 20084

FOUNDATIONS FOR COMPUTER SIMULATION OF A
LOW PRESSURE OIL FLOODED SINGLE SCREW
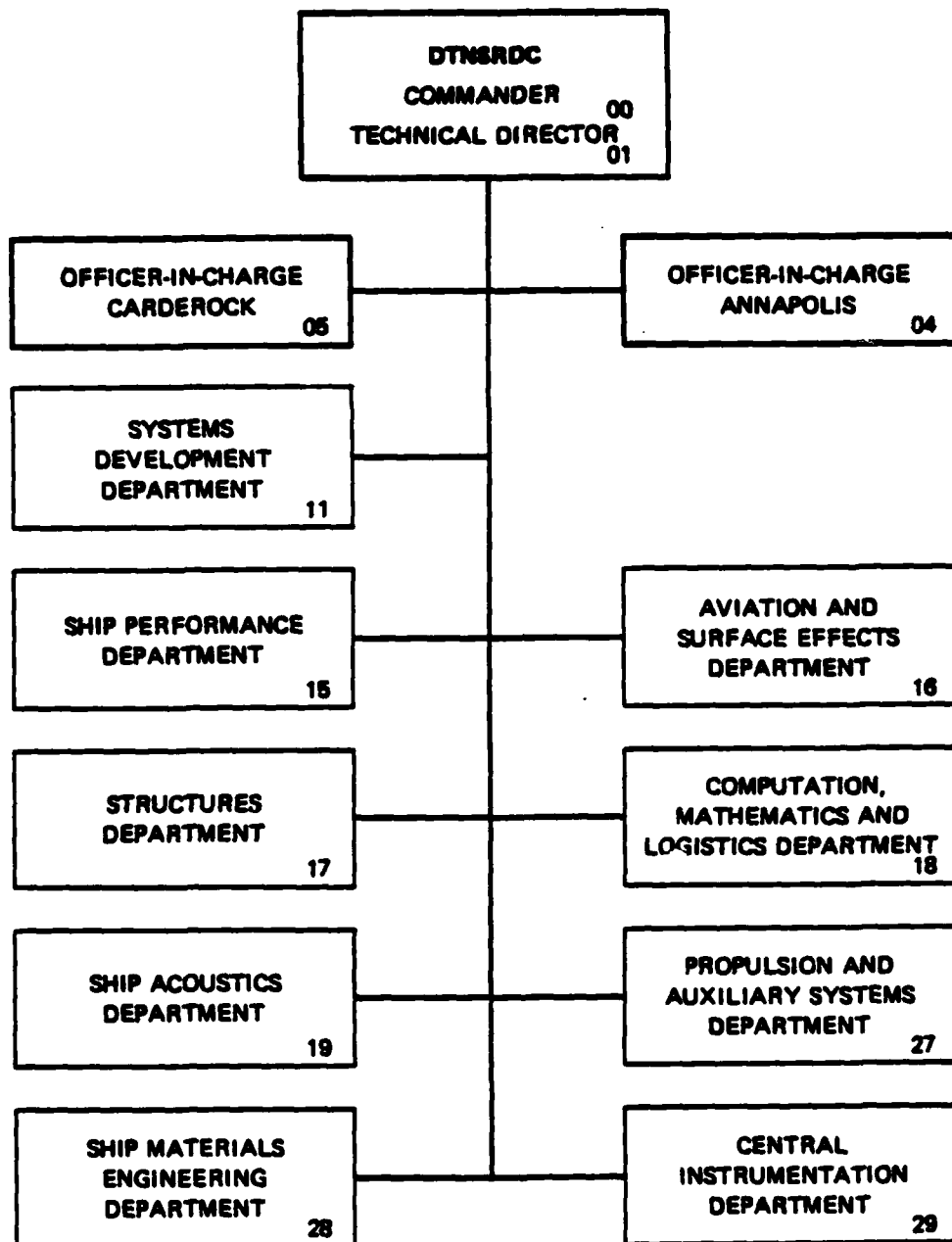AIR COMPRESSOR

by

Thomas W. Bein

DTIC
SELECTED
DEC 8 1981

H

APPROVED FOR PUBLIC RELEASE; DISTRIBUTION UNLIMITED

PROPULSION AND AUXILIARY SYSTEMS DEPARTMENT
RESEARCH AND DEVELOPMENT REPORT

81 12 08196

MAJOR DTNSRDC ORGANIZATIONAL COMPONENTS

```
                    ┌─────────────────────────┐
                    │        DTNSRDC          │
                    │      COMMANDER          │
                    │                    00   │
                    │ TECHNICAL DIRECTOR      │
                    │                    01   │
                    └─────────────────────────┘
                                 │
   ┌──────────────────────┐             ┌──────────────────────┐
   │  OFFICER-IN-CHARGE    │             │  OFFICER-IN-CHARGE    │
   │    CARDEROCK          │             │    ANNAPOLIS          │
   │                05     │             │                04     │
   └──────────────────────┘             └──────────────────────┘

   ┌──────────────────────┐
   │     SYSTEMS           │
   │   DEVELOPMENT         │
   │   DEPARTMENT          │
   │                11     │
   └──────────────────────┘

   ┌──────────────────────┐             ┌──────────────────────┐
   │  SHIP PERFORMANCE     │             │   AVIATION AND        │
   │   DEPARTMENT          │             │   SURFACE EFFECTS     │
   │                15     │             │   DEPARTMENT          │
   │                      │             │                16     │
   └──────────────────────┘             └──────────────────────┘

   ┌──────────────────────┐             ┌──────────────────────┐
   │    STRUCTURES         │             │   COMPUTATION,        │
   │   DEPARTMENT          │             │   MATHEMATICS AND     │
   │                17     │             │  LOGISTICS DEPARTMENT │
   │                      │             │                18     │
   └──────────────────────┘             └──────────────────────┘

   ┌──────────────────────┐             ┌──────────────────────┐
   │   SHIP ACOUSTICS      │             │  PROPULSION AND       │
   │   DEPARTMENT          │             │  AUXILIARY SYSTEMS    │
   │                19     │             │   DEPARTMENT          │
   │                      │             │                27     │
   └──────────────────────┘             └──────────────────────┘

   ┌──────────────────────┐             ┌──────────────────────┐
   │   SHIP MATERIALS      │             │    CENTRAL            │
   │   ENGINEERING         │             │  INSTRUMENTATION      │
   │   DEPARTMENT          │             │   DEPARTMENT          │
   │                28     │             │                29     │
   └──────────────────────┘             └──────────────────────┘
```

REPORT DOCUMENTATION PAGE	READ INSTRUCTIONS BEFORE COMPLETING FORM

1. REPORT NUMBER DTNSRDC/PAS-81/24	2. GOVT ACCESSION NO. AD A108230	3. RECIPIENT'S CATALOG NUMBER

4. TITLE (and Subtitle) FOUNDATIONS FOR COMPUTER SIMULATION OF A LOW PRESSURE OIL FLOODED SINGLE SCREW AIR COMPRESSOR	5. TYPE OF REPORT & PERIOD COVERED Research & Development
	6. PERFORMING ORG. REPORT NUMBER

7. AUTHOR(s) Thomas W. Bein	8. CONTRACT OR GRANT NUMBER(s)

9. PERFORMING ORGANIZATION NAME AND ADDRESS David W. Taylor Naval Ship R&D Center Bethesda, MD 20084	10. PROGRAM ELEMENT, PROJECT, TASK AREA & WORK UNIT NUMBERS Work Unit 2722-142

11. CONTROLLING OFFICE NAME AND ADDRESS Naval Sea Systems Command (SEA 5321) Washington, DC 20362	12. REPORT DATE December 1981
	13. NUMBER OF PAGES 119

14. MONITORING AGENCY NAME & ADDRESS(if different from Controlling Office)	15. SECURITY CLASS. (of this report) UNCLASSIFIED
	15a. DECLASSIFICATION/DOWNGRADING SCHEDULE

16. DISTRIBUTION STATEMENT (of this Report) APPROVED FOR PUBLIC RELEASE; DISTRIBUTION UNLIMITED

17. DISTRIBUTION STATEMENT (of the abstract entered in Block 20, if different from Report)

18. SUPPLEMENTARY NOTES Prepared as a Masters Degree Thesis for Purdue University, West Lafayette, Indiana.

19. KEY WORDS (Continue on reverse side if necessary and identify by block number) Compressor Thermodynamics Fluid Dynamics

20. ABSTRACT (Continue on reverse side if necessary and identify by block number)

    The necessary logic to construct a computer model to predict the performance of an oil flooded, single screw air compressor is developed. The geometric variables and relationships used to describe the general single screw mechanism are developed. The governing equations to describe the processes are developed from their primary relationships. The assumptions used in the development are also defined and justified.

(Continued on reverse side)

DD FORM 1473 1 JAN 73   EDITION OF 1 NOV 65 IS OBSOLETE
S/N 0102-LF-014-6601

(Block 20 continued)

The computer model predicts the internal pressure, temperature, and flowrates through the leakage paths throughout the compression cycle of the single screw compressor. The model uses empirical external values as the basis for the internal predictions. The computer values are compared to the empirical values, and conclusions are drawn based on the results. Recommendations are made for future efforts to improve the computer model and to verify some of the conclusions that are drawn.

Acces
NTI
DT
Un
Just

By
Di
Av   Code
            /or
Dist   .

A

TABLE OF CONTENTS

LIST OF FIGURES

NOMENCLATURE

English Symbols

a	Leakage path clearance
A	Cross sectional area discharge port path
Area	Plane area of star tooth engaged in main rotor, cross sectional area of leakage path
b	Slope of angle plate in leakage path
cl	Clearance between plates
c_p	Specific heat at constant pressure
c_v	Specific heat at constant volume
C	Degrees Centigrade - absolute
dm	Rate of mass flow
dU	Rate of change of internal energy
dV	Rate of volume change
D	Hydraulic diameter
DVRATIO	Ratio of volume in thread before suction closure

f	Friction factor
F	Correction factor
h	Fluid enthalpy
h_L	Head loss
k	Ratio of specific heats
K	Resistance coefficient
KPa	Kilo Pascals - absolute
L	Throttling length of leakage path
L_1	Length of unequal throttling length
L_1'	Length of divided unequal throttling length
L_2	Length of unequal throttling length
L_2'	Length of divided unequal throttling length
m	Mass
$\dot{m}$	Mass rate of flow
n	Polytropic exponent
NM	Number of threads in main rotor
NS	Number of star teeth

NSTARS   Number of star rotors

P Pressure - absolute

$\dot{Q}$ Volumetric flowrate

r Pressure ratio

r_c Critical pressure ratio

$\bar{r}$ r coordinate location of centroid of star tooth area

R Gas constant

R Radial component in cylindrical coordinates

R_e Reynolds number

RI   Star rotor inner radius

RM   Main rotor radius

RMRSH   Radius of main rotor shaft

RS   Star rotor outer radius

T Temperature - absolute

U Internal energy, velocity of moving plate

v Specific volume

V Fluid velocity

Volume   Volume swept out of main rotor

w   Width of star tooth, width of leakage path

X   Orthogonal axis

Y   Orthogonal axis

Z   Orthogonal axis

Greek Symbols

α Inlet heat transfer coefficient

δQ Differential Quantity of heat transferred
          to control volume

δW Differential Quantity of work done to
          control volume

ΔL Change in throttling length

ΔP Pressure gradient

$\Delta \theta_{MR}$ Angle increment of main rotor

ν Kinematic viscosity of fluid

ρ Mass density

θ_{chord} One half of chord length of intersection of
          the star rotor and the outside diameter of
          the main rotor

θ_{MRINJ} — Angle where oil injection begins, relative to suction closure

θ_{STINR} — Angle between inside corner points of star tooth

θ_{STOUTR} — Angle between outside corner points of star tooth

θ_{STSC} — Star rotor angle where main rotor closes suction port

θ_{STAR} — Angle of centerline of star tooth

θ_{STASC} — Total angle star tooth will rotate through from suction closure until tooth pulls out of main rotor

Subscripts

1 — Initial value

2 — Final value

c — Corrected value

cv — Value in control volume

CVI — Control volume I

disch — Value in discharge plenum

DP — Discharge plenum condition

ent — Value at entrance to leakage path

exit   Value at exit to leakage path

hi   Values at high pressure side of convergent divergent path

I   Inlet condition

in   Into control volume

lo   Values at low pressure side of convergent divergent path

mid   Values where slope changes in convergent divergent path

n   Value at beginning of time step

n+1   Value at end of time step

n+g   Value at end of time step due to geometry

out   Out of control volume

p   Predicted value

ABSTRACT

The necessary logic to construct a
computer model to predict the performance of
an oil flooded, single screw air compressor
is developed. The geometric variables and
relationships used to describe the general
single screw mechanism are developed. The
governing equations to describe the processes
are developed from their primary
relationships. The assumptions used in the
development are also defined and justified.

The computer model predicts the internal
pressure, temperature, and flowrates through
the leakage paths throughout the compression
cycle of the single screw compressor. The
model uses empirical external values as the
basis for the internal predictions. The
computer values are compared to the empirical
values, and conclusions are drawn based on
the results. Recommendations are made for
future efforts to improve the computer model
and to verify some of the conclusions that
are drawn.

ADMINISTRATIVE INFORMATION

INTRODUCTION

The single screw compressor is a rotary, positive dis-
placement, oil-flooded, compressor. Although a U.S. Patent
was issued to Chilton in 1952 for a similar mechanism,
Bernard Zimmern, President of Omphale S.A. Paris, France,
is credited with the developments and techniques used in
the present day machines. Single screw compressors are
presently commercially produced for air and refrigeration
compressor service. The single screw mechanism has
balanced pressure forces acting on the main rotor, which
results in low bearing loads and the elimination of prob-
lems associated with rotor deflection.

The use of computer models to simulate a process have
gained widespread acceptance. In some cases, computer models
are used to provide information on the internal conditions
of a process by using some known external values. In other
cases, the computer model is used to make predictions on the
effect of a change in the design. The use of a computer
model, as an aid in the design of a component, can result in
significant savings because building prototypes, to evaluate
a design, is expensive and time consuming. However,
construction of a dependable and versatile computer model
is also expensive. The cost of the computer model is

most times recovered quickly by changes in the design that result in improved performance.

This thesis covers the development of a computer model that will attempt to predict the internal pressure, temperature, and flowrates through the leakage paths, of a single screw air compressor. The computer model will use empirical external values as the basis for the internal predictions. The empirical values were determined by testing an oil flooded single screw air compressor*. The available data is the flowrates, temperatures, and pressures, that were measured at the intake and discharge of the compressor.

The single screw compressor gets its name from the one main rotor instead of the two rotors that are used in the twin screw compressor. There is a thread cut into the main rotor, as shown in Figure 1. The thread is cut so that a tooth on the side rotor, referred to as the star rotor, can travel through the main rotor thread. The star tooth is analogous to the piston in a reciprocating compressor and the main rotor thread would be the cylinder.

The compression process begins by filling the thread with suction air. The suction flow is axial through the open end of the main rotor. When the thread is filled with air, a star tooth meshes with the main rotor, and closes the

---

* The compressor air end was part of an air compressor package manufactured by the Chicago Pneumatic Tool Company, Franklin, PA.

Figure 1.
Single Screw Air Compressor

suction port. The air is confined by the sides of the main rotor thread, the star tooth, and, the housing that is a close fit to the main rotor. The air is compressed until the main rotor thread uncovers the discharge port that is located in the housing. When the discharge port is opened, the air flows radially out of the main rotor thread into the discharge plenum. As the star tooth sweeps out the main rotor thread, compressing the air, the thread is filling on the bottom side of the star tooth. The star tooth on the other side of the main rotor then engages the same main rotor thread, and the process repeats.

As mentioned previously, the single screw compressor used in this evaluation is an oil flooded type. The oil acts as a coolant, lubricant, and sealant. The amount of oil injected has a significant effect on the performance of the single screw compressor. The oil is injected into the main rotor thread, beginning when the star closes the suction port, and continuing until the thread passes the injection orifice.

The objective of this task is to gain additional understanding of the processes that occur within the single screw air compressor. The approach used, is to develope a computer model of the compressor that will predict the process based on external empirical values. The describing relationships will be developed from basic laws and equations. The assumptions that are made will be defined and justified.

The results of the computer model will be compared to the empirical data, and conclusions will be drawn.

GEOMETRY

INDEPENDENT VARIABLES

There are seven primary independent variables required to define a particular star and main rotor combination. These are:

NM   = Number of threads in main rotor.

NS   = Number of star teeth.

NSTARS = Number of star rotors.

RI   = *Star rotor inner radius.*

RM   = Main rotor radius.

RS   = *Star rotor outer radius.*

w   = *Width of star tooth.*

When these variables are defined, the following physical constraints should be kept in mind:

1.)   The number of threads in the main rotor, NM, should be a multiple of the number of star rotors, NSTARS. This is so that the radial pressure forces acting on the main rotor will be balanced. When the number of threads is a multiple of the number of star rotors, the pressure developed in a pocket will be the same as the pressure developed in a pocket being closed by another star rotor.

2.)   The number of threads in the main rotor, NM, and the
number of star teeth should not have common factors so that
each star tooth will mesh with every main rotor thread.
This will serve to maintain uniform clearances as the
machine wears.

3.)   At the point of suction closure, the thread to be
swept must not extent beyond the plane of the next star
rotor. In this way the thread is allowed to fill completely
with suction gas before it is closed and the compression
process begins.

The geometric relationship for this constraint can be
developed beginning with Figure 2.   For the main rotor,
cylindrical coordinates are positioned so that the Z axis is
coincident with the main rotor axis and so that the origin
is at a point where a line perpendicular to the main rotor
axis, the X axis, intersects the star rotor axis. The star
rotor is also defined by cylindrical coordinates.   The Z
axis is positioned so that it is coincident with the star
rotor axis and the X axis is coincident with the X axis from
the main rotor coordinates. A point on the star rotor will
rotate in the X Z plane defined by the main rotor coordi-
nates.

The angle θ_{chord} is one half of the chord length and is
expressed by:
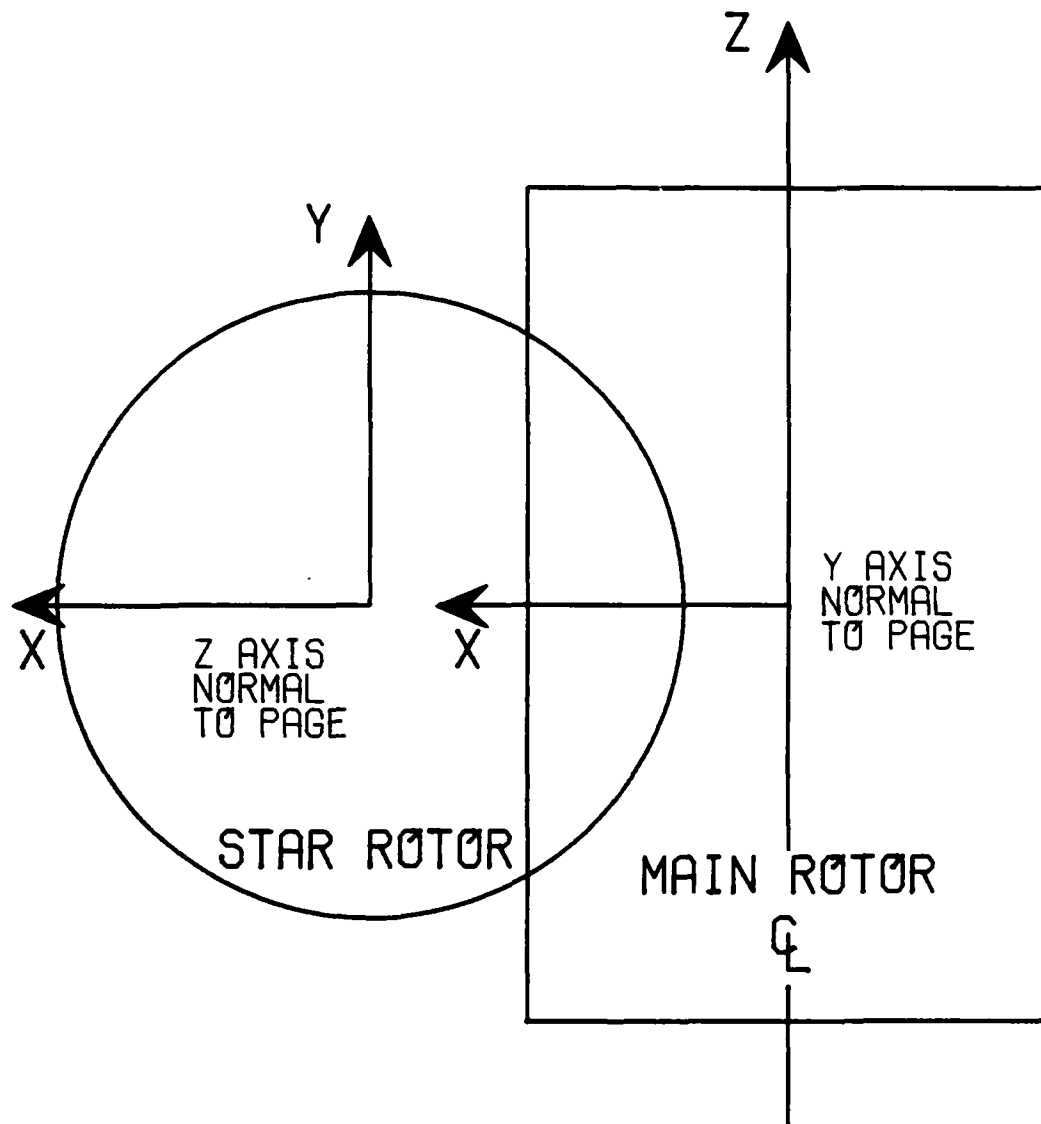
$$\theta_{chord} = Arccos \left[\frac{RI}{RS}\right]$$

Figure 2.
Coordinate Definition

The angle where the main rotor closes the suction port is a secondary independent variable. This is shown as θ_{STSC} on Figure 3. The total angle that the star tooth will rotate through after suction closure, θ_{STASC}, is the sum of θ_{STSC}, θ_{chord} and one half of the angle between the outer corners of a star tooth, θ_{STOUTR}, Figure 4. The main rotor angular rotation is related by the ratio of NS and NM. The angle that the thread wraps around the main rotor from suction closure must be less than 2π / NSTARS. This is expressed as:

$$\theta_{STASC} \left[\frac{NS}{NM}\right] < \frac{2\pi}{NSTARS}$$

4.) The depth of star rotor penetration into the main rotor must be less than that which would cut into the main rotor shaft. If the radius of the main rotor shaft is RMRSH, this can be expressed as:

$$RM-(RS-RI) > RMRSH$$

5.) The number and width of teeth specified for the star rotor must be capable of fitting on a circle of radius RI. Referring to Figure 4, the angle between the inner corners of the star finger, θ_{STINR}, can be determined by:

$$\theta_{STINR} = 2 \text{ Arcsin}\left[\frac{W}{2RI}\right]$$

In order that all of the star teeth will fit on the specified circle the following must be satisfied:
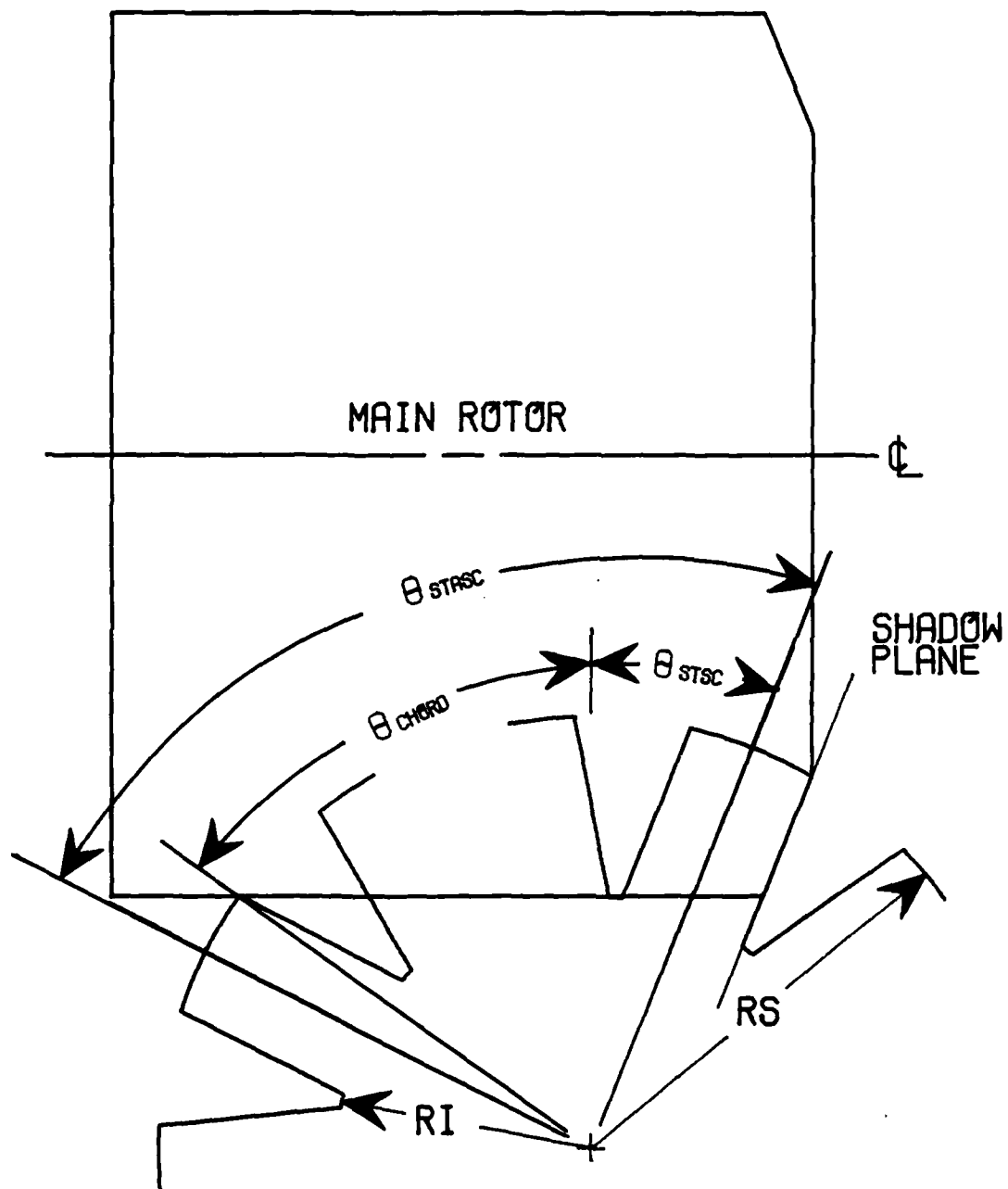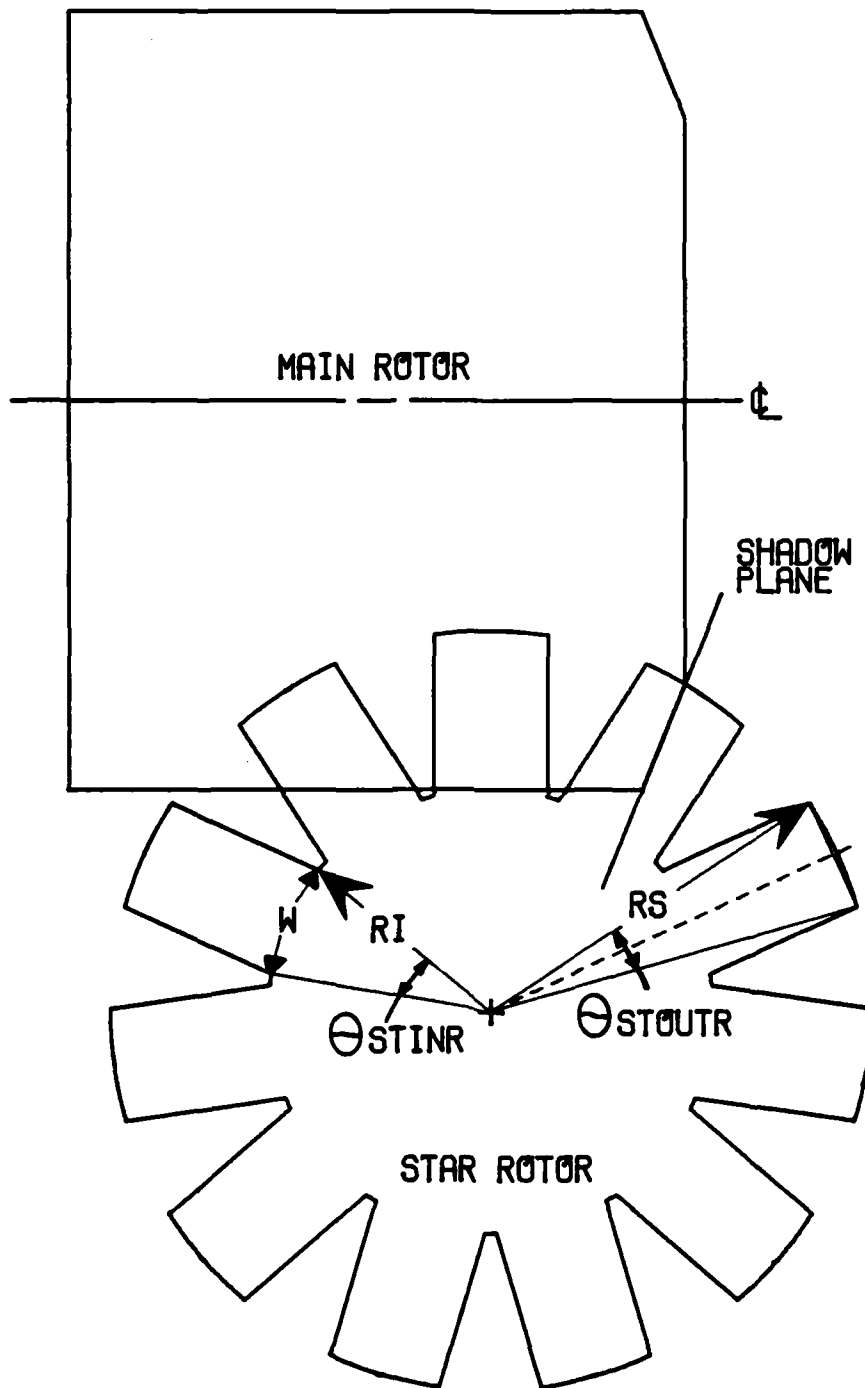
Figure 3.
Star Rotor Angle Definitions

Figure 4.
Star Rotor Tooth Angles

$$\theta_{STINR} < \frac{2\pi}{NS}$$

Variables that do not define the geometry but establish "limits" will be referred to as secondary variables. These are:

θ_{STSC} = Star tooth centerline angle at suction closure.

θ_{MRINJ} = Main rotor angle, relative to suction closure, where oil injection begins.

DVRATIO = Ratio of volume in thread before suction closure to volume in thread when discharge begins.

The first of these, θ_{STSC}, is a factor used to determine how far the thread to be swept wraps around the main rotor at suction closure. Changing the point of suction closure has the obvious effect of changing the swept volume, but there are two other parameters dependent on where suction closure is positioned. They are: the pressure in the thread at the point of suction closure and the size of the axial suction port. These will be discussed further in the discussion of the suction process.

The second variable, θ_{MRINJ}, establishes when the leading thread of the main rotor will begin to uncover the oil injection port. When oil injection begins before suction closure, oil takes up volume in the thread which reduces the amount of gas that can be delivered. However, if injection is delayed too long the volumetric efficiency drops, because across some leakage paths, air is leaking instead of oil.

The third variable, DVRATIO, controls where the leading thread will uncover the discharge port. This controls the final part of the pressure curve. If the discharge port opens too early, there will be undercompression and higher losses across the leakage paths. If the discharge port opens too late, there will be overcompression and again higher losses across the leakage paths.

APPLICATION

The corners of the star rotor can be expressed in terms of the main rotor coordinates z and r. Referring to Figure 5, the leading flank of the tooth is the side between points 1 and 2, the tip is between 2 and 3, the trailing flank is between 3 and 4, and the window is between 4 and 1. The coordinates of the points 1 and 4 are determined by finding the z location of where the centerline passes through the outside diameter of the main rotor and adding or subtracting the distance from the centerline to the flank. This is expressed as:

$$z(1) = RI \ TAN(\theta_{STAR}) + \frac{W}{2}/COS(\theta_{STAR})$$
$$z(4) = RI \ TAN(\theta_{STAR}) - \frac{W}{2}/COS(\theta_{STAR})$$

r (1) and r (4) are simply equal to RM. The coordinates of the points 2 and 3 are expressed as:

$$z(2) = RS \ SIN(\theta_{STAR} + \theta_{STOUTR})$$
$$r(2) = RM + RI - RS \ COS(\theta_{STAR} + \theta_{STOUTR})$$

Figure 5.
Star Rotor Point Notation

$$z(3) = RS \ SIN(\theta_{STAR} - \theta_{STOUTR})$$

$$r(3) = RM + RI - RS \ COS(\theta_{STAR} - \theta_{STOUTR})$$

Recalling that the star rotor angular position is related to the main rotor rotation, the paths that the flanks make while progressing through the main rotor can be produced in a planar representation, Figure 6. The solid lines are on the outside surface of the main rotor and the dashed lines are the paths described by the corners of the star tip. It is emphasized that in this format the main rotor axis is normal to the plane of the paper.

The volume of the thread is determined by calculating the volume swept by the star tooth. The star tooth shape is defined by the corner points, plus sufficient points between 2 and 3, to describe the star tooth tip shape. The tooth area and the r coordinate of the location of the centroid , $\bar{r}$, of the area are expressed by the following from Wojciechowski [1].*

$$Area = \sum_{i=0}^{n} (z_{i+1} - z_i)(r_{i+1} + r_i)/2$$

$$\bar{r} = \frac{1}{Area} \sum_{i=0}^{n} [(z_{i+1} - z_i)/8][(r_{i+1} + r_i)^2 + (r_{i+1} - r_i)^2/3]$$

To determine the volume of the main rotor thread a theorem by Pappus is used. This states that:

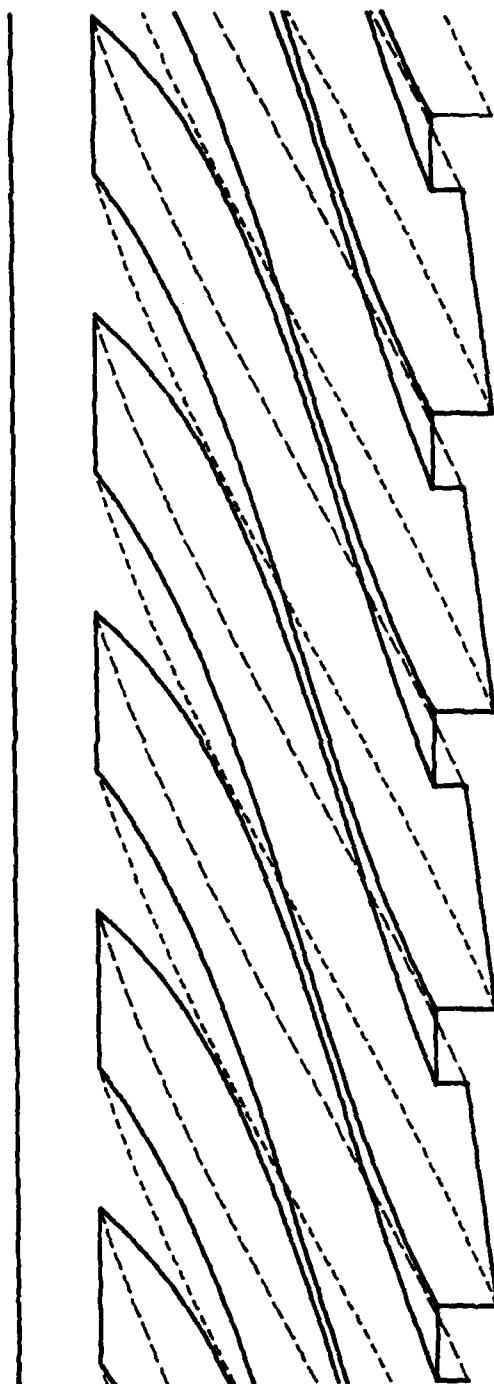* The number in brackets refers to the list of references.

Figure 6.
Planar Main Rotor Plot

If a planar area is revolved about an axis in its plane, but not intersecting the area, the volume of the surface of revolution so formed is equal to the product of the area and the length of the path traced by the centroid of the area.[2]

$$\text{Volume} = \text{Area } \Delta\theta_{MR}\bar{r}$$

The following dimensions will be used to define the CY6-40 Compressor:

DVRATIO = 3.6

NM   = 6

NS   = 11

NSTARS = 2

RI   = 5.011 cm

RM   = 8.738 cm

RS   = 8.575 cm

w   = 2.570 cm

θ_{MRINJ} = -16 deg

θ_{STSC} = -22 deg

The following figures were made by substituting these values into the appropriate relationships. Figure 7 is the incremental volume versus main rotor angle. The points where the suction port closes and where the discharge port opens are indicated. The portion of the curve between where the main rotor angle is equal to zero and suction closure uses a modified version of the area relation. This is to model the suction process and will be discussed further in the section dealing with the suction process. Figure 8 is
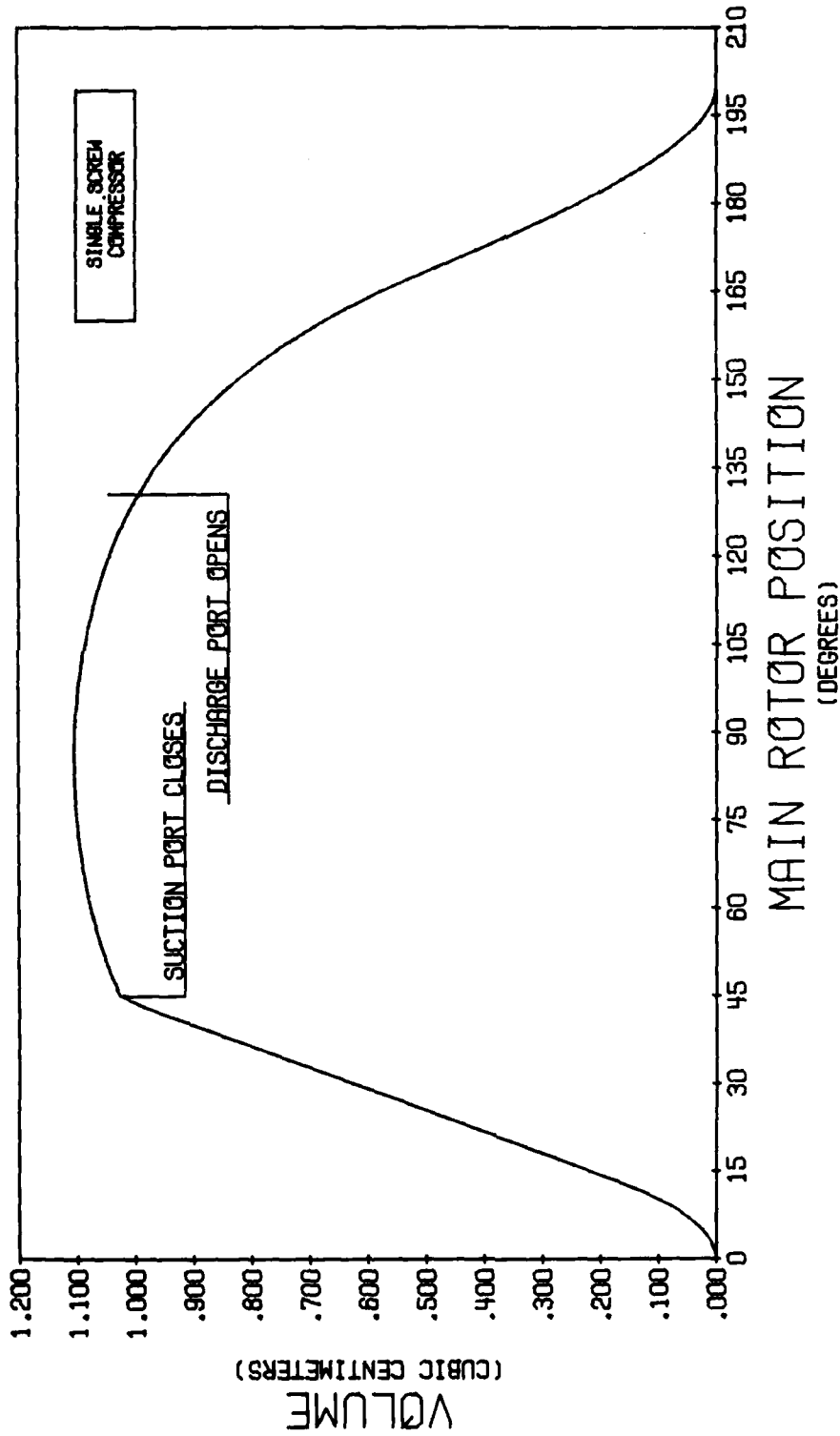
Figure 7.
Incremental Volume

the swept volume versus main rotor angle. The upper line is the cumulative swept volume from the beginning of the compression process. The lower line is the cumulative swept volume from suction closure. The lengths of the star tooth leading edge, tip, and trailing edge, are shown in Figures 9, 10, and 11 respectively.
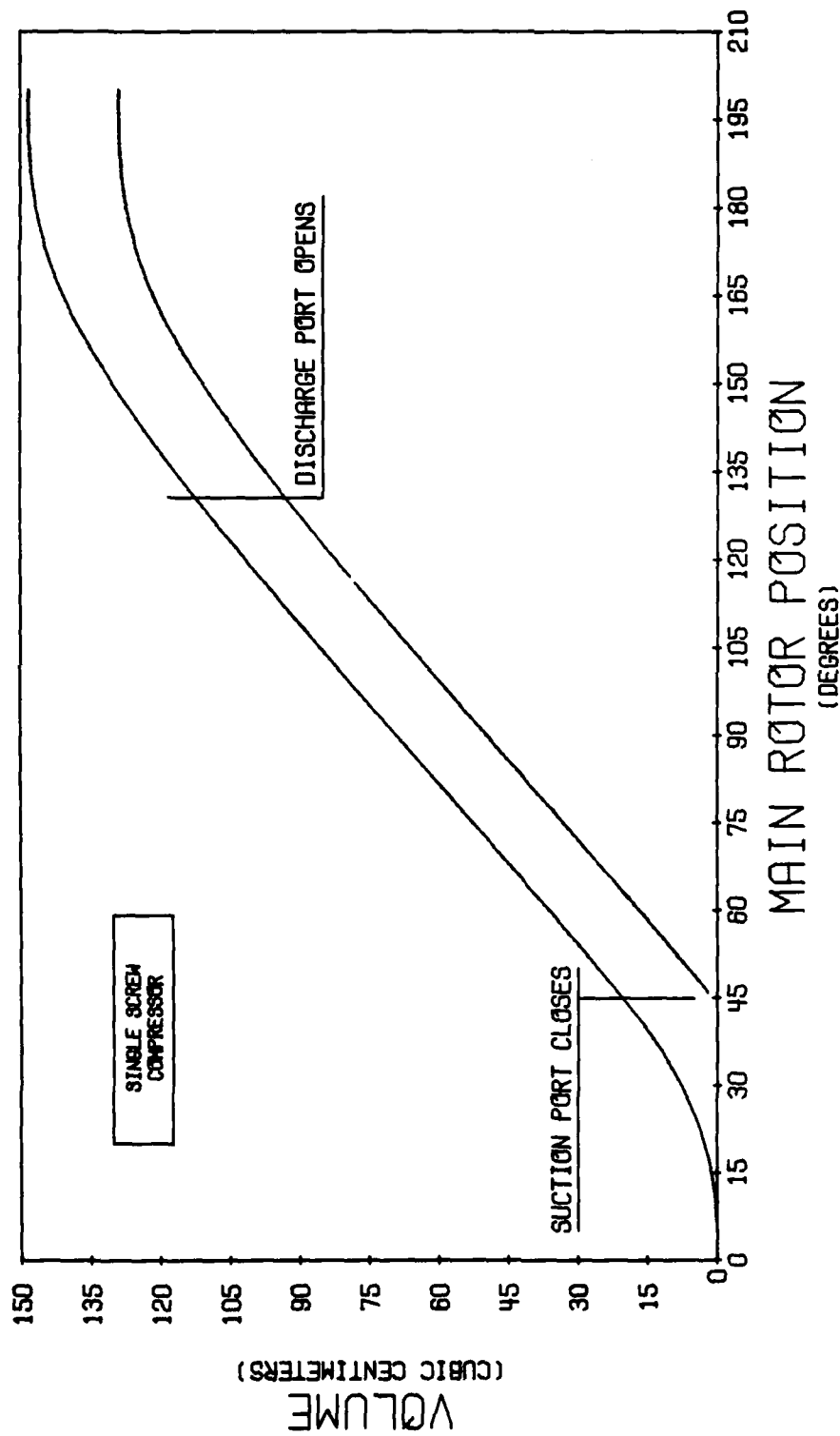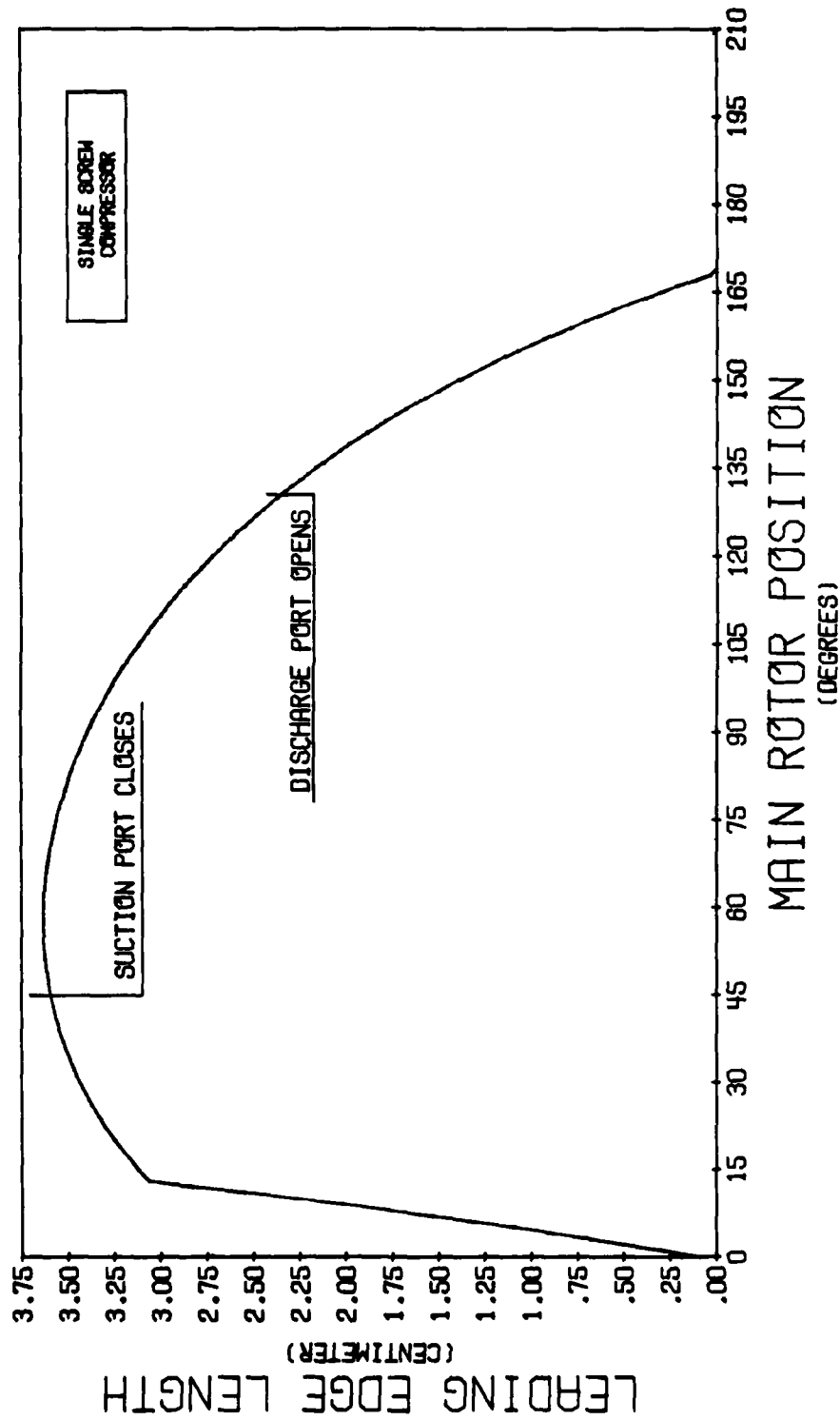
Figure 8.
Cummulative Volume

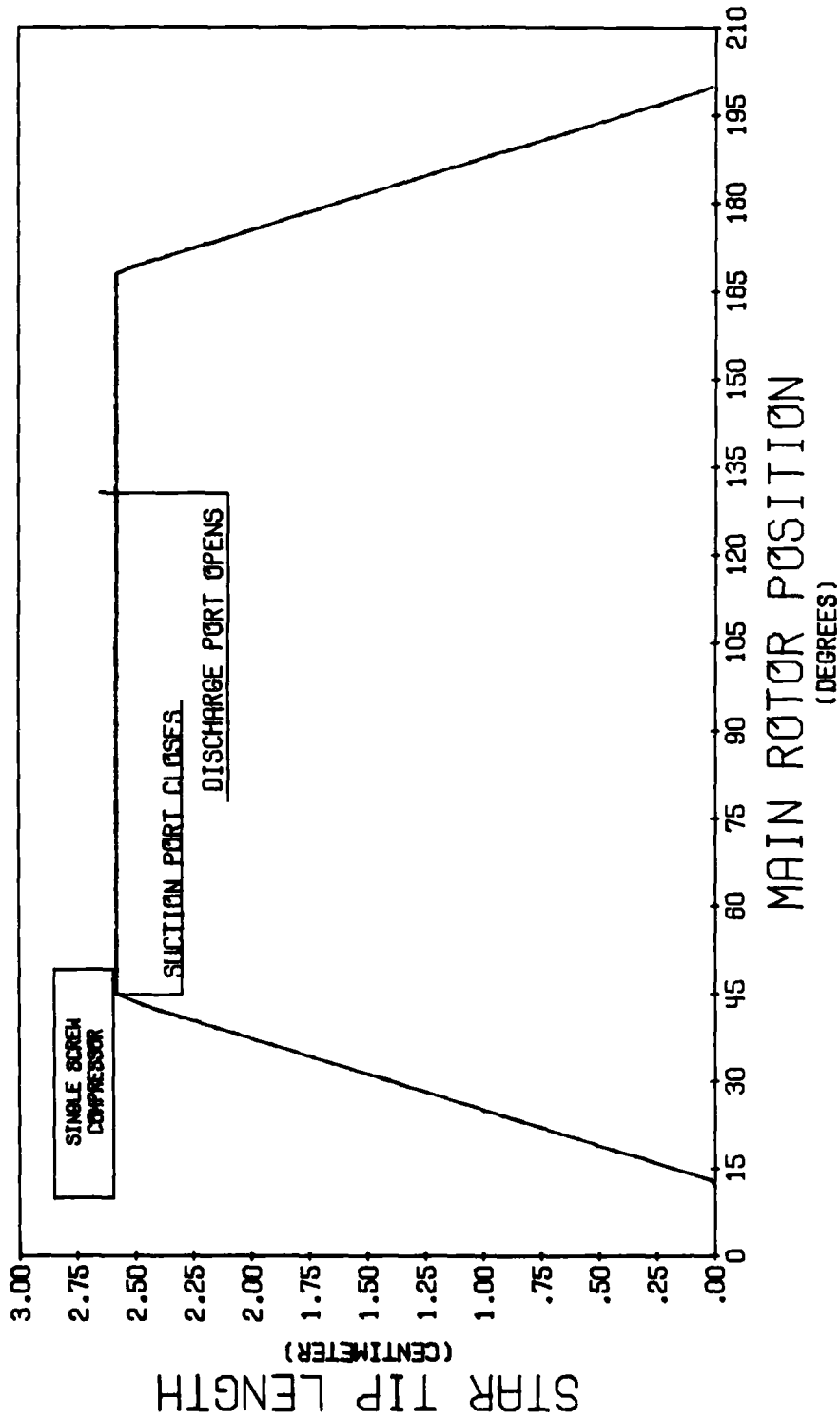Figure 9.
Star Tooth Leading Flank Length

Figure 10.
Star Tooth Tip Length

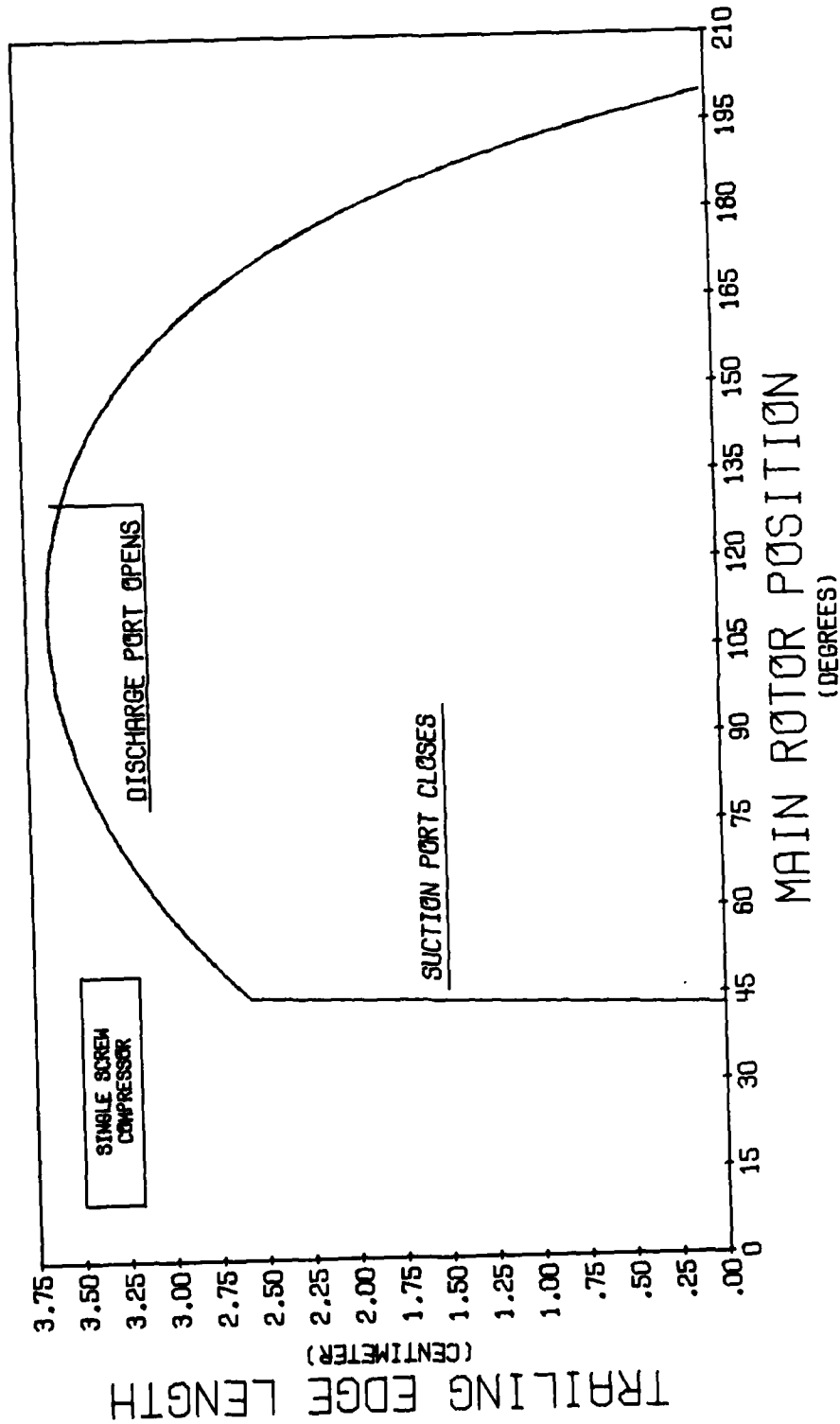Figure 11.
Star Tooth Trailing Flank Length

PROCESS DESCRIPTION

CONVENTION

The compression process begins with charging the thread in the main rotor with suction air. Because of the large inlet port, and the decreasing volume increment as the star tooth pulls out of the main rotor, the losses across the inlet port will be assumed to be negligible. The suction closure cycle will then be taken as starting when the star rotor leading flank first comes in contact with the main rotor. The main rotor thread, from this point until the star rotor trailing flank closes with the main rotor trailing thread, will be denoted as control volume I, Figure 12.

The compression part of the cycle begins when the star rotor trailing flank closes the main rotor thread. The main rotor thread from this point until the star rotor leaves the main rotor will be denoted as control volume II. Figure 13 shows the beginning of control volume II and an intermediate position. Control volume II will then have a closed compression process and a process where a boundary of the control volume is open to the discharge plenum via the discharge port.
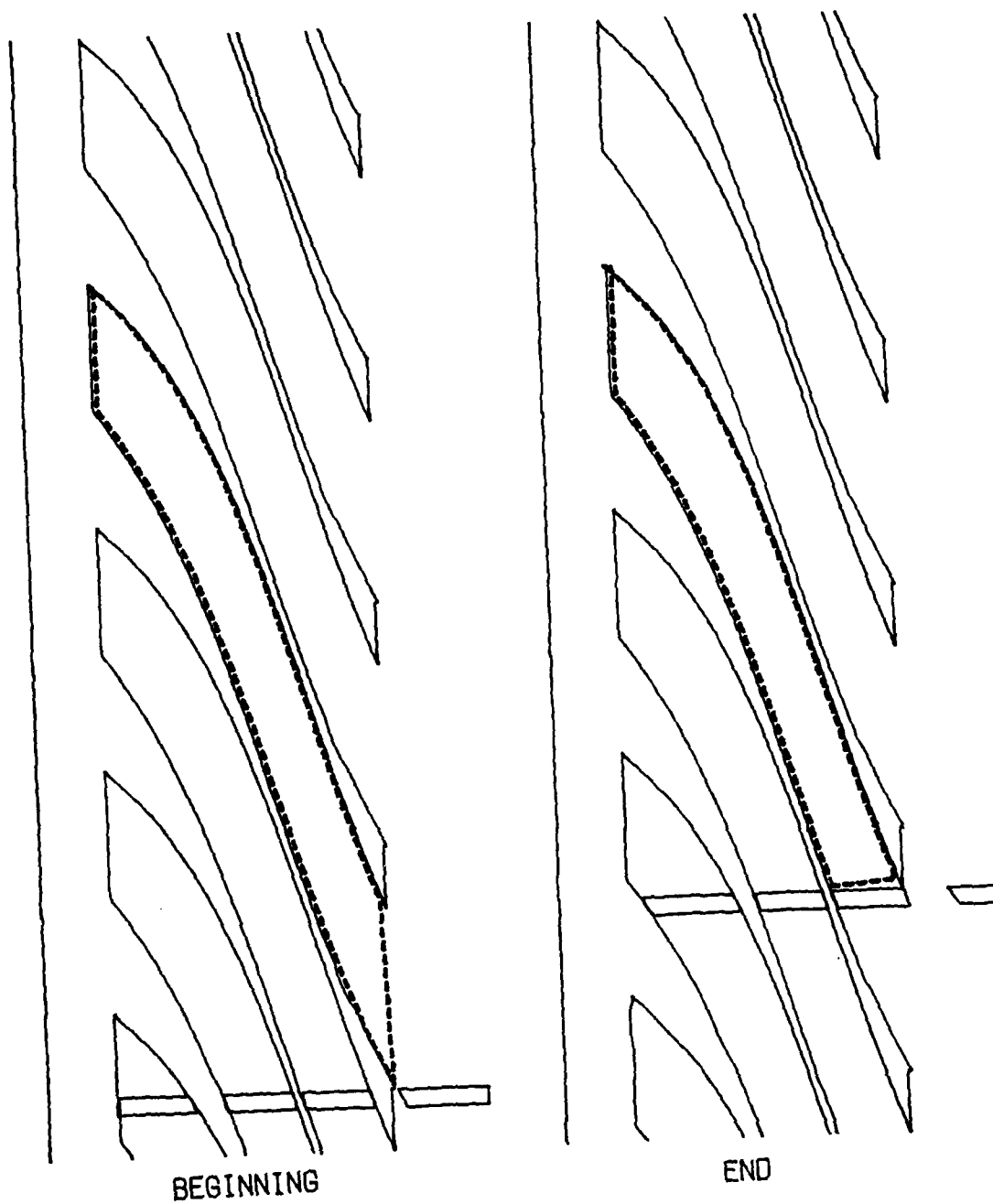
BEGINNING   END

Figure 12.
Boundaries of Control Volume I

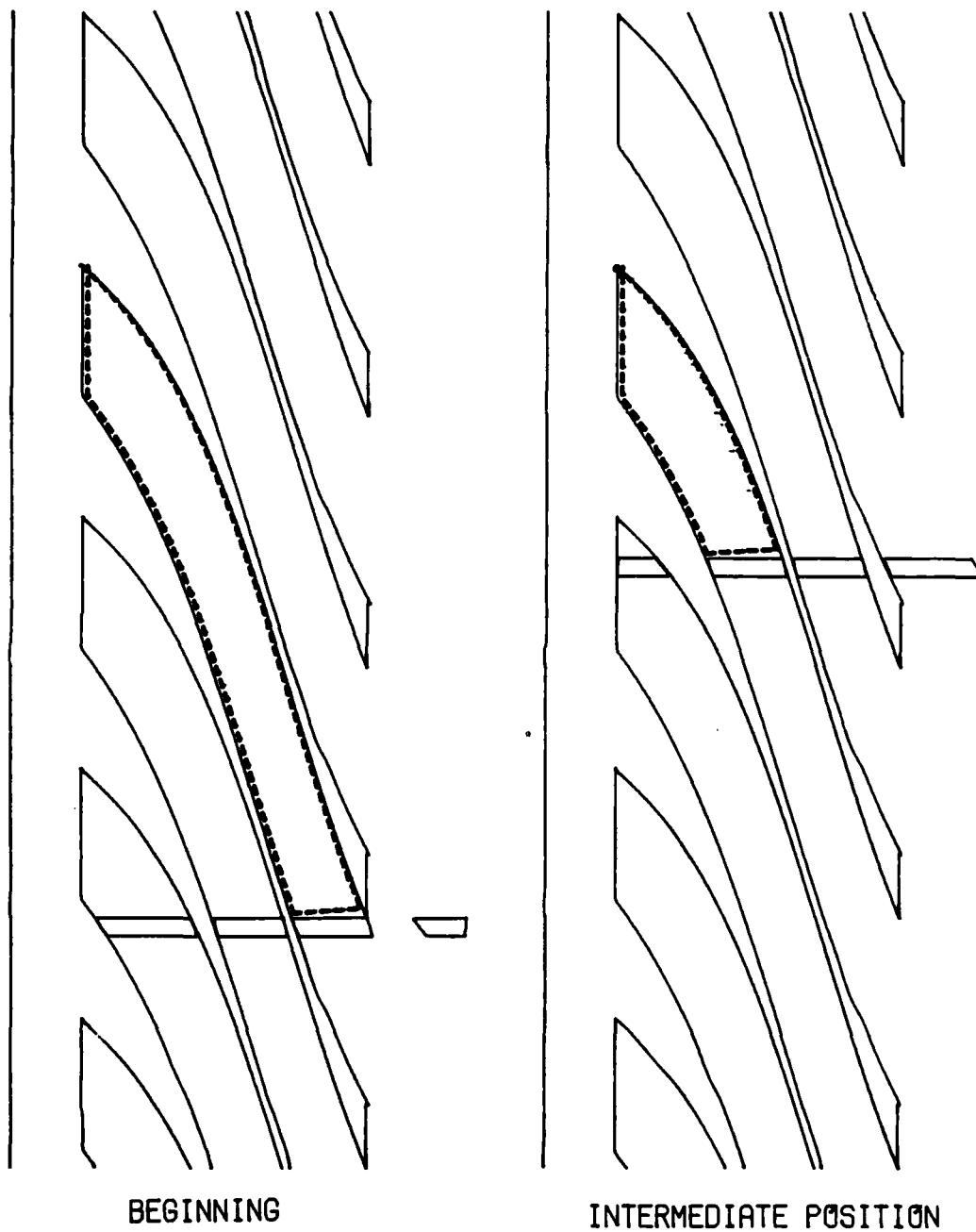BEGINNING   INTERMEDIATE POSITION

Figure 13.
Boundaries of Control Volume II

In order to provide a clear visualization of the geometry, the following format will be used. The main rotor will be presented in planar form, with the star rotor of the particular thread being discussed, shaded in as shown in Figure 14. Also shown, will be a plan view of the star rotor with the same star tooth shaded in. Recalling that the star rotor intersects the main rotor in a plane, the additional star teeth will also be shown but not shaded in. The discharge port will also be shown just above the plane of the star rotor with the one side positioned so that it is parallel with the leading thread of the main rotor, just prior to when the discharge port opens. The threads on the main rotor will be shown as being stationary and the plane of the star rotor will be moved to indicate the subsequent positions. The leading thread will be considered as the thread ahead of the thread being discussed and conversely for the trailing thread.

The following assumptions will be made for the analysis:

1.) The air behaves as an ideal gas.

2.) The properties within the control volume are uniform.

3.) Gravitational and kinetic energies are neglected.

4.) Inlet air is preheated to a uniform temperature before entering thread.

5.) Frictional losses across the inlet port are negligible.
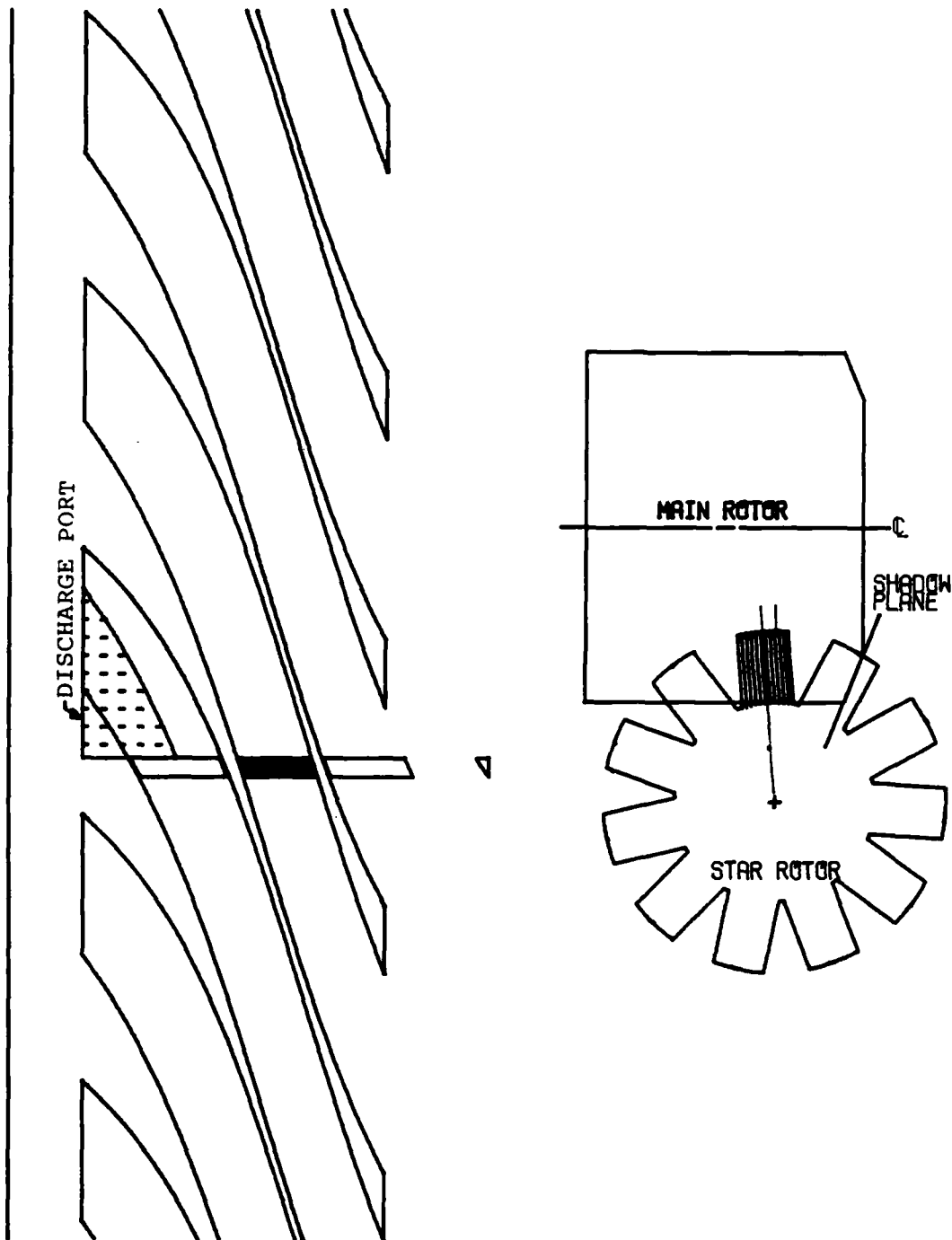
DISCHARGE PORT

MAIN ROTOR

SHADOW PLANE

STAR ROTOR

Figure 14.
Presentation Convention for the
Star Rotor and Main Rotor

6.) Pressures and temperatures in the suction and discharge plenums are constant.

7.) The values predicted for one thread will be the same as the values in the other threads when the appropriate phase angle is accounted for.

8.) There will not be any air leaking across the leakage paths within the control volumes.

9.) Any oil that leaves control volume II that goes either directly into control volume I or into an area connected to the suction chamber will be assumed to go into control volume I.

10.) There will not be any backflow of oil into the control volume when the discharge port opens and the discharge pressure is higher than the pressure in control volume II.

11.) The heat transferred between the air in the compression chamber and the oil will be negligible.

12.) The heat transfer between the air and the oil passing through the discharge port will be assumed to continue until they will maintain thermal equilibrium.

SUCTION CLOSURE PROCESS

The boundaries of control volume I were introduced in Figure 12. The boundary that is across the open end of the thread will be taken to be a plane that includes the star rotor trailing flank at suction closure and is perpendicular to the star rotor plane. In this way it can be considered to be the shadow of the main rotor on the star rotor. Figure 15 shows the position of the main rotor and of the star rotor at the beginning of the suction process. Figure 16 is the position at the end of the suction closure process.

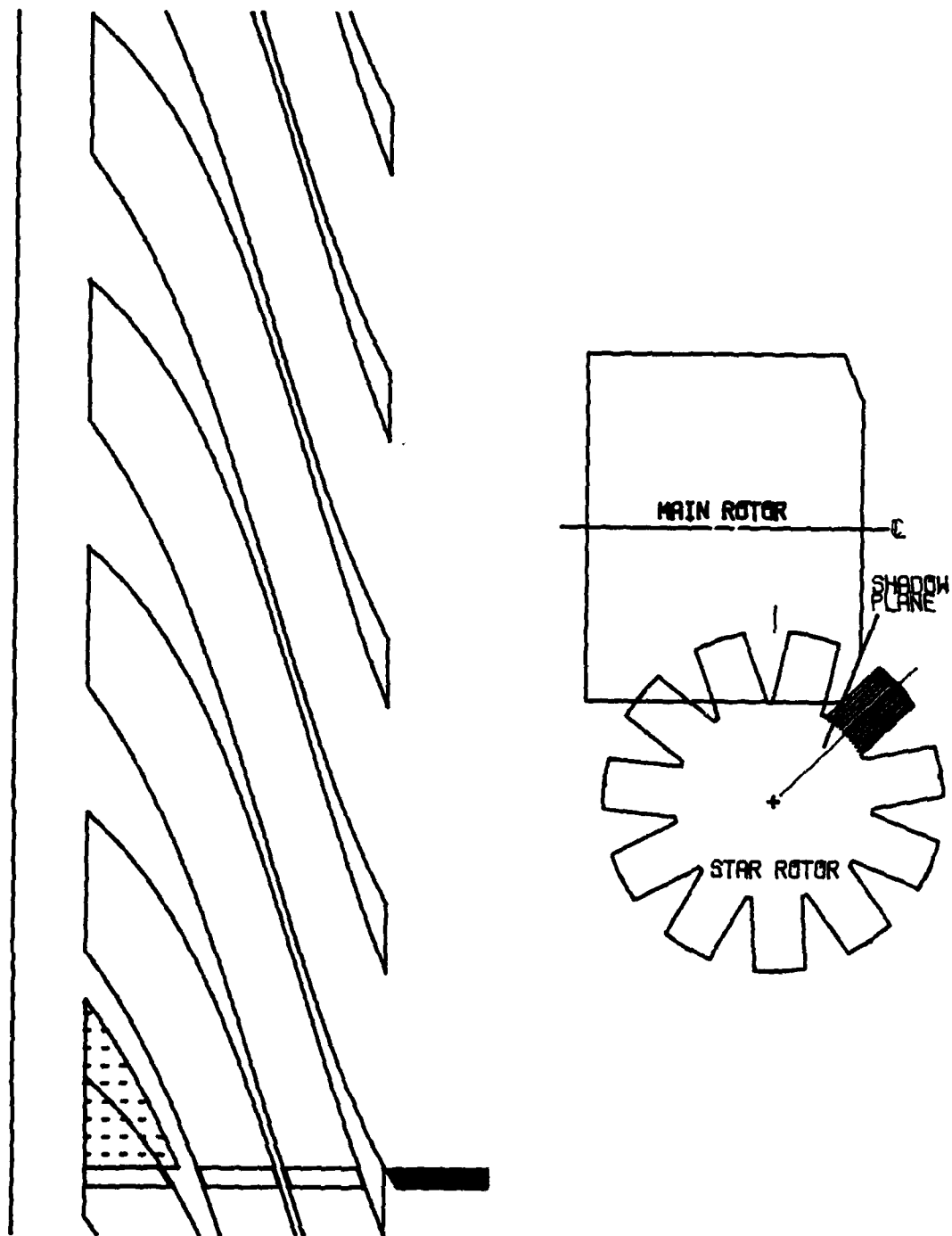The governing energy equation will be the first law of thermodynamics.

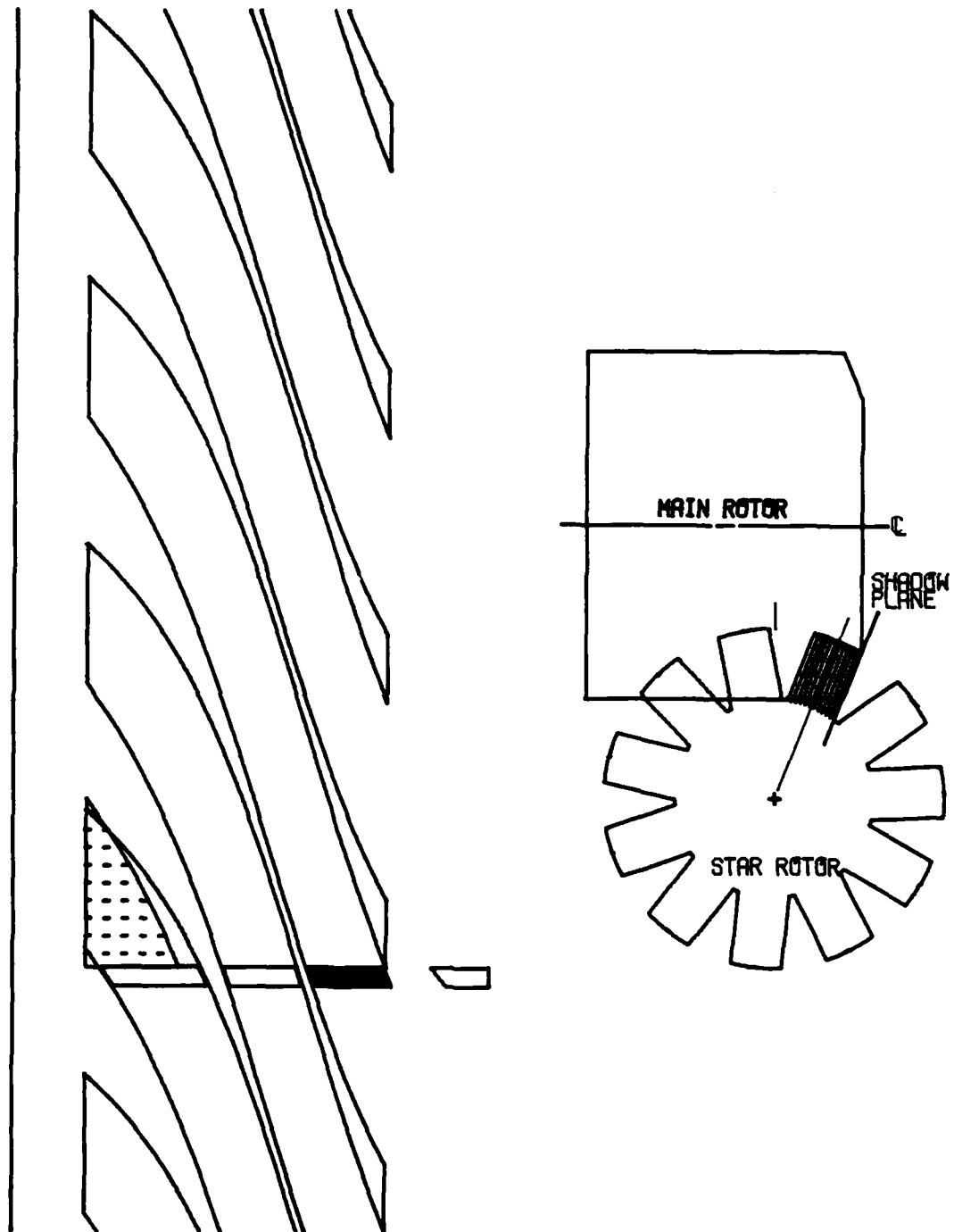Figure 15.
Beginning of Suction Process

Figure 16.
End of Suction Process

$$\delta Q - \delta W + h_{in} dm_{in} - h_{out} dm_{out} = dU_{cv} \qquad (1)$$

Where:

δQ = Differential quantity of heat transferred to the control volume - positive for heat into control volume.

δW = Differential quantity of work done to the control volume - positive for work out of control volume.

h_{in} = Enthalpy of suction gas.

dm_{in} = Rate of suction air flow into control volume.

h_{out} = Enthalpy of gas in control volume.

dm_{out} = Rate of air flow discharging from control volume.

dU_{cv} = Rate of change of internal energy in control volume.

The volume of control volume I is being reduced, therefore, there will not be any air flow into it; $dm_{in} = 0$. The air temperature is assumed constant, so the heat transferred will be zero. Rewriting:

$$-\delta W_{cv} - h_{out} dm_{out} = dU_{cv}$$

The work can be written as:

$$\delta W_{cv} = P_{cv} dV_{cv}$$

Where:

P_{cv} = Pressure in the control volume.

dV_{cv} = Rate of change of volume in the control volume.

From the assumption that the properties within the control volume are uniform, and if the specific enthalpy of the control volume is denoted by h_{cv}, then $h_{out}=h_{cv}$. Due to conservation of mass, the rate of mass flow out of the control volume is equal to the rate of change of mass in the control volume, dm_{cv}. Thus:

$$-P_{cv}dV_{cv}-h_{cv}dm_{cv}=dU_{cv} \qquad (2)$$

Assuming constant specific heats, the specific enthalpy and internal energy can be expressed by:

$$U_{cv}=c_v T_{cv}$$
$$h_{cv}=c_p T_{cv}$$

Where:

c_v = Specific heat at constant volume.

c_p = Specific heat at constant pressure.

T_{cv} = Temperature in control volume.

The total internal energy is the product of the specific internal energy and the mass. Therefore:

$$dU_{cv}=m_{cv}c_v dt_{cv}+c_v T_{cv}dm_{cv}$$

But, the temperature in this process is assumed to be constant, so:

$$dU_{cv}=c_v T_{cv}dm_{cv}$$

Substituting into equation (2) and solving for P_{cv}:

$$P_{cv} = \frac{T_{cv} dm_{cv}(c_p - c_v)}{dV_{cv}}$$

Recognizing that:

$$R = c_p - c_v$$

Where R is the gas constant. Then:

$$P_{cv} = \frac{T_{cv} R dm_{cv}}{dV_{cv}} \tag{3}$$

The mass rate of flow of air out of the control volume, dm_{cv}, is evaluated by applying Bernoulli's equation. Solving for V, and simplifying, this is written:

$$V = \sqrt{\frac{2 \, \Delta P}{\rho}} \tag{4}$$

Where ΔP is the pressure gradient across the inlet port, and ρ is the mass density. This is subject to the following assumptions:

1.)   Steady flow

2.)   Frictionless

3.)   Flow along a streamline

4.)   Incompressible flow

For this application the flow is considered to be steady during the time increment. The flow is frictionless and along a streamline. Furthermore, the flow is considered to be incompressible because of the small change in pressure.

The rate of change of the volume is a function of the geometry and of the oil flow rate in and out of the control volume via the leakage paths. Equation (3) is solved by incrementing through the cycle and by employing a predictor-corrector scheme. The new pressure is predicted by reducing the volume by the geometric volume increment between the time steps. This is written:

$$P_p = \frac{T_{cv} R m_n}{V_{n+g}}$$

Where:

P_p = The predicted pressure.

T_{cv} = Temperature in control volume - constant

m_n = Mass in control volume at beginning of increment.

V_{n+g} = Available volume in control volume at end of increment due to geometry.

This predicted pressure is then used to evaluate the mass flow of air and the mass flow of oil during the time increment. Due to the incompressibility of the oil, the mass flow of oil can be related to a volume change. ΔP, ρ, and P are quantities that are required to evaluate the mass flow rates that change during the increment. To account for this, the average of the values at the beginning and end of the increment are used. The relationship for corrected pressure is written:

$$P_c = \frac{T_{cv} R \, m_c}{V_c}$$

Where:

P_c = The corrected pressure at n+1.

V_c = The corrected volume at n+1.

m_c = The corrected mass of air at n+1.

If the difference between P_p and P_c is above a tolerance limit, the procedure is repeated by setting P_p equal to P_c. Figure 17 is a conceptual plot of pressure versus volume for this procedure showing two iterations.

The other case that is encountered when evaluating the pressure of control volume I during the suction closure process is when the corrected pressure is less than the pressure in the suction chamber. This is a result of the large inlet port and the predicted pressure. This case is physically unrealistic and can be corrected in a few ways. These are to take smaller time steps, to correct the predicted pressure so that the pressure at the end of the step is suction pressure, or to simply assume the pressure in the control volume remained constant during the increment. The last alternative was chosen because it is representative of the real process and is simpler than the other approaches.

CLOSED COMPRESSION PROCESS

The closed compression process, control volume II, begins when the beginning of the main rotor trailing thread
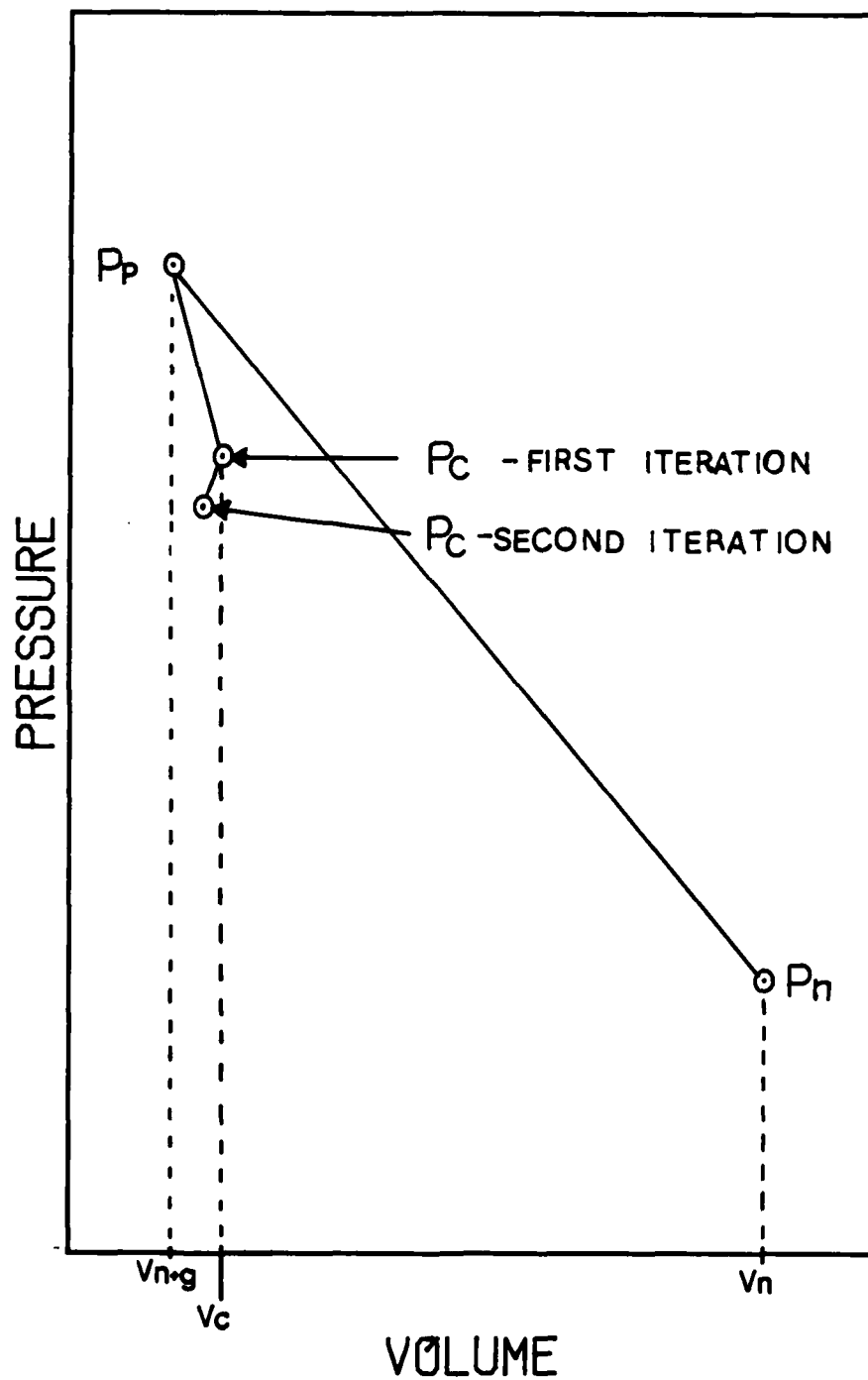
Figure 17.
Predictor Corrector Scheme for the
Suction Process

meets the star rotor trailing flank, thereby closing the inlet port. The closed compression process ends when the leading thread of the main rotor overlaps the trailing edge of the discharge port. The star rotor and main rotor positions at the beginning and end of the closed compression process are shown in Figure 18 and Figure 19 respectively. The only openings in the boundaries of control volume II are the leakage paths. By assumption, only oil passes through these, so the mass of air in the control volume is constant.

There is assumed to be no heat transfer between the air and the oil while in the control volume. This is supported by the idea that the process occurs too quickly for the oil to absorb a significant amount of heat from the compressed air. As a consequence of this assumption, it is recognized that at the air-oil interface, a thin film of oil will be approximately at the same temperature as the air. This is much higher than the temperature of the air-oil mixture after it leaves the compressor. This idea has been shown to be the case by information from operating compressors. When oil was used that was suitable for the discharging air-oil mixture temperature, but not suitable for significantly higher temperatures, premature oil degradation was found. This indicates that at some point in the cycle a portion of the oil was exposed to temperatures higher than that of the discharging air-oil mixture.
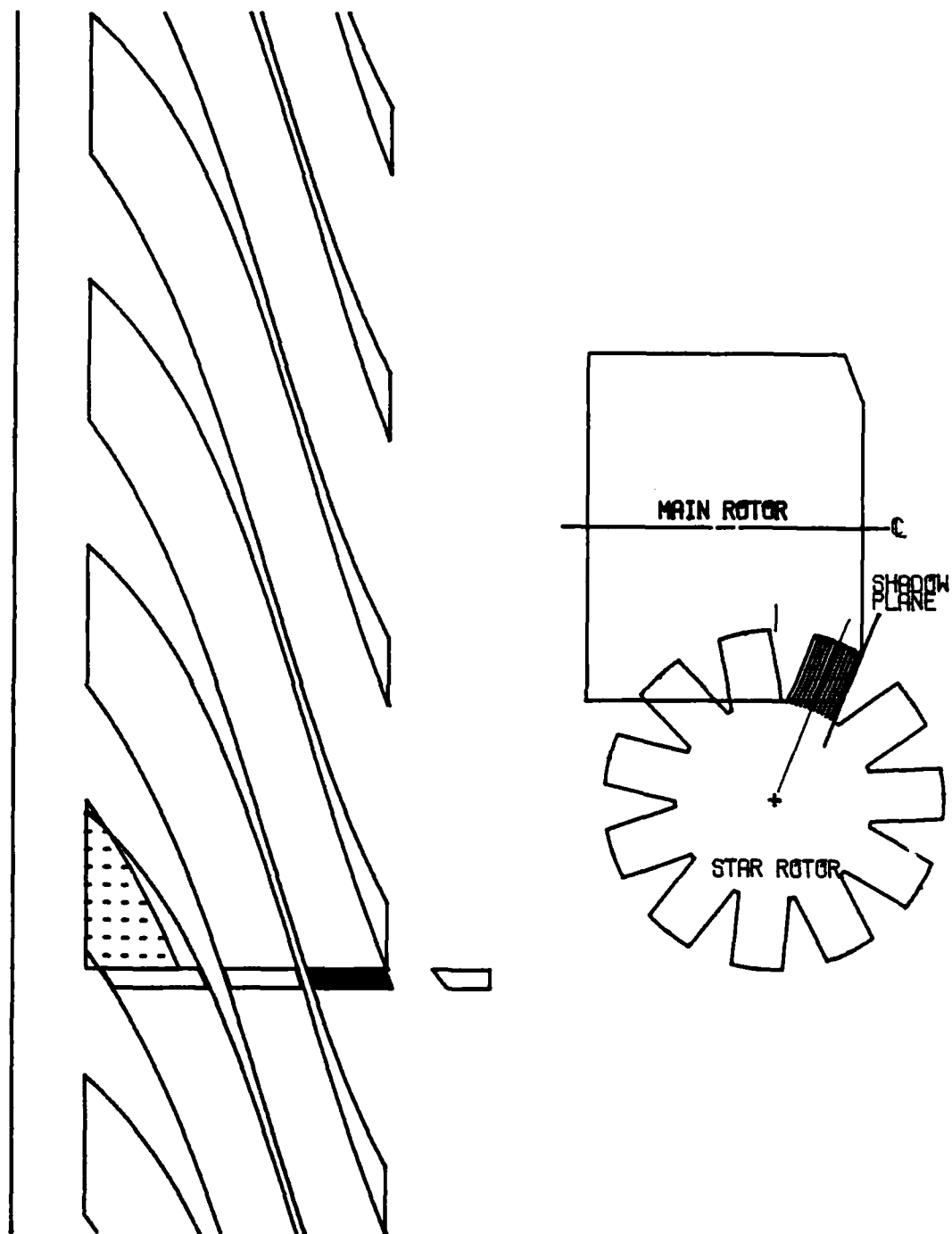
The governing energy equation is the first law of

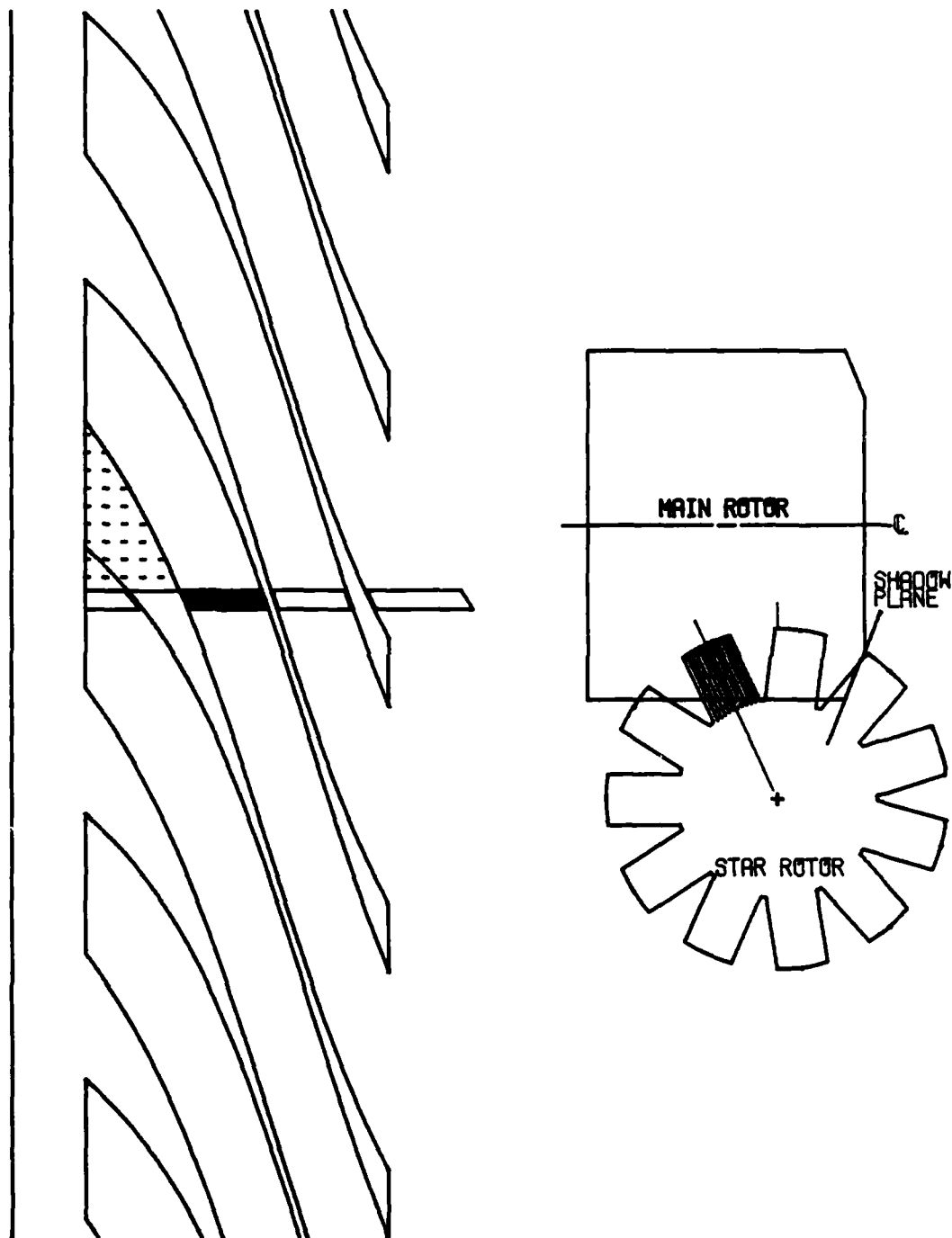Figure 18.
Beginning of Closed Compression Process

Figure 19.
End of Closed Compression Process

thermodynamics for a closed process:

$$\delta Q - \delta W = dU$$

From this relationship, it can be developed that for an isentropic process:

$$Pv^k = \text{Constant}$$

Where:

P = Pressure

v = Specific volume

k = Ratio of specific heats

If the heat transfer from the air being compressed was known to be small compared to the work of the control volume this relationship could be applied. However, the heat transferred from the air is not known. Therefore, the equation for a polytropic process will be used. Where n is the polytropic exponent:

$$Pv^n = \text{Constant}$$

The value of n will be determined by matching known temperature points from data on a compressor with values predicted from this process relationship. The temperature of the air-oil mixture is known after discharge from the thread. The value of n will be determined by assuming a value for n and incrementing through the process. At the end of the closed compression process, the temperature that

the mass of air and oil, at their associated temperatures, contained in the control volume would reach if allowed to go to equilibrium will be computed. This temperature will then be compared to the known temperature of the mixture at discharge. If the predicted temperature is not within a tolerance limit of the known point, a secant method interpolation is used to predict a new value of n. This procedure is repeated until the predicted temperature is within the tolerance limit set.

The pressure of the control volume is determined with a similar predictor- corrector scheme as in the discussion of the suction closure process. In this case, the polytropic relation and the predicted pressure will be used and is written as:

$$P_p = P_n (V_n / V_{n+g})^n$$

Where:

P_n = The pressure at the beginning of the increment.

V_n = Available volume of control volume II at beginning of increment.

V_{n+g} = Available volume of control volume II at end of increment due to geometry.

The predicted pressure is used to evaluate the mass flow of oil through each of the leakage paths. The volume available to the air at the end of the increment is equal to the original volume plus the geometric increment plus the volume due to oil flow. This is written:

$$P_c = P_n(V_n/V_{n+1})^n$$

Where V_{n+1} is the volume available to the air at the end of the increment. Obviously, the pressure varies during the increment. The mass flows of oil need the pressure of the control volume for the calculation. To compensate for the changing pressure an average pressure during the time increment is used by the mass flows of oil.

The predictor-corrector procedure is repeated until the difference between the predicted and corrected pressure is below a tolerance limit. When the limit has been satisfied, the temperature of the air is found from the ideal gas relation. This is written:

$$T_{n+1} = \frac{P_{n+1}V_{n+1} R}{m_{cv}}$$

Where:

T_{n+1} = Air temperature at the end of the increment.

P_{n+1} = Pressure in control volume at the end of the increment.

DISCHARGE PROCESS

The discharge process, control volume II, begins when the leading thread of the main rotor overlaps the trailing edge of the discharge port. The discharge process ends when the star rotor trailing flank disengages from the main rotor. The star rotor and main rotor positions at the beginning and end of the discharge process are shown in

Figure 20 and Figure 21 respectively. The discharge port opens control volume II to the discharge plenum.

Again, it is assumed that only oil passes through the leakage paths in the boundary of the control volume. When the pressure in the control volume is less than the discharge plenum pressure, only air will be considered to flow into the control volume. There will not be any heat transfer between the air and oil in the control volume. Also, the discharge plenum pressure and temperature will be assumed to be constant and the heat transferred to the surroundings from flow through the discharge port will be assumed to be negligible. Finally, the discharge process will be considered to be the combination of closed volume compression, and flow either in or out of a rigid vessel.

For the closed volume compression, the polytropic relationships described in the closed compression process will be used to generate predicted values of the pressure and temperature in control volume II at the end of the increment due to geometric volume change. The polytropic exponent n will be the value that was iterated for during the closed compression process. These relations are:

$$P_p = P_n (V_n/V_{n+g})^n$$
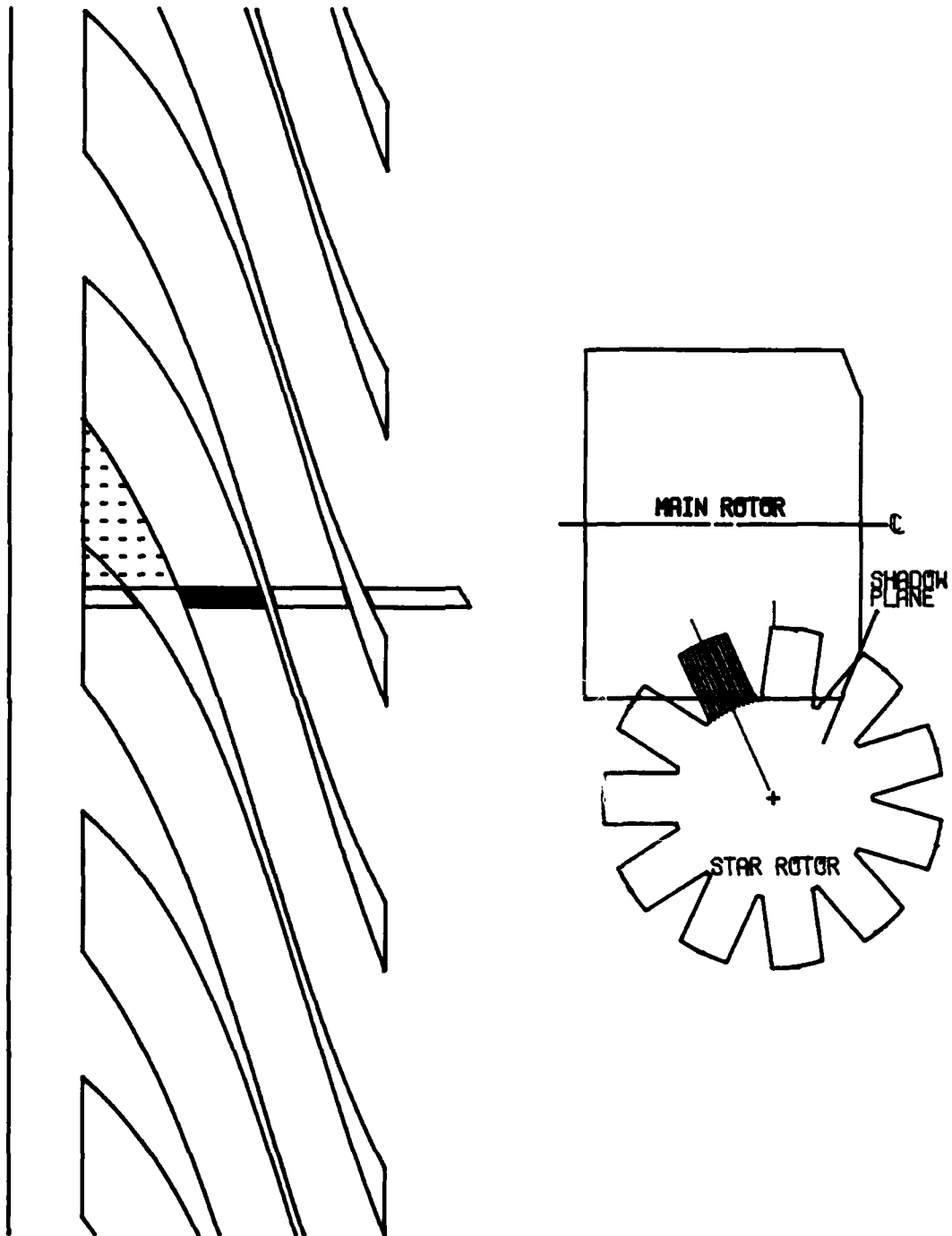$$T_p = T_n (V_n/V_{n+g})^n$$

Where:

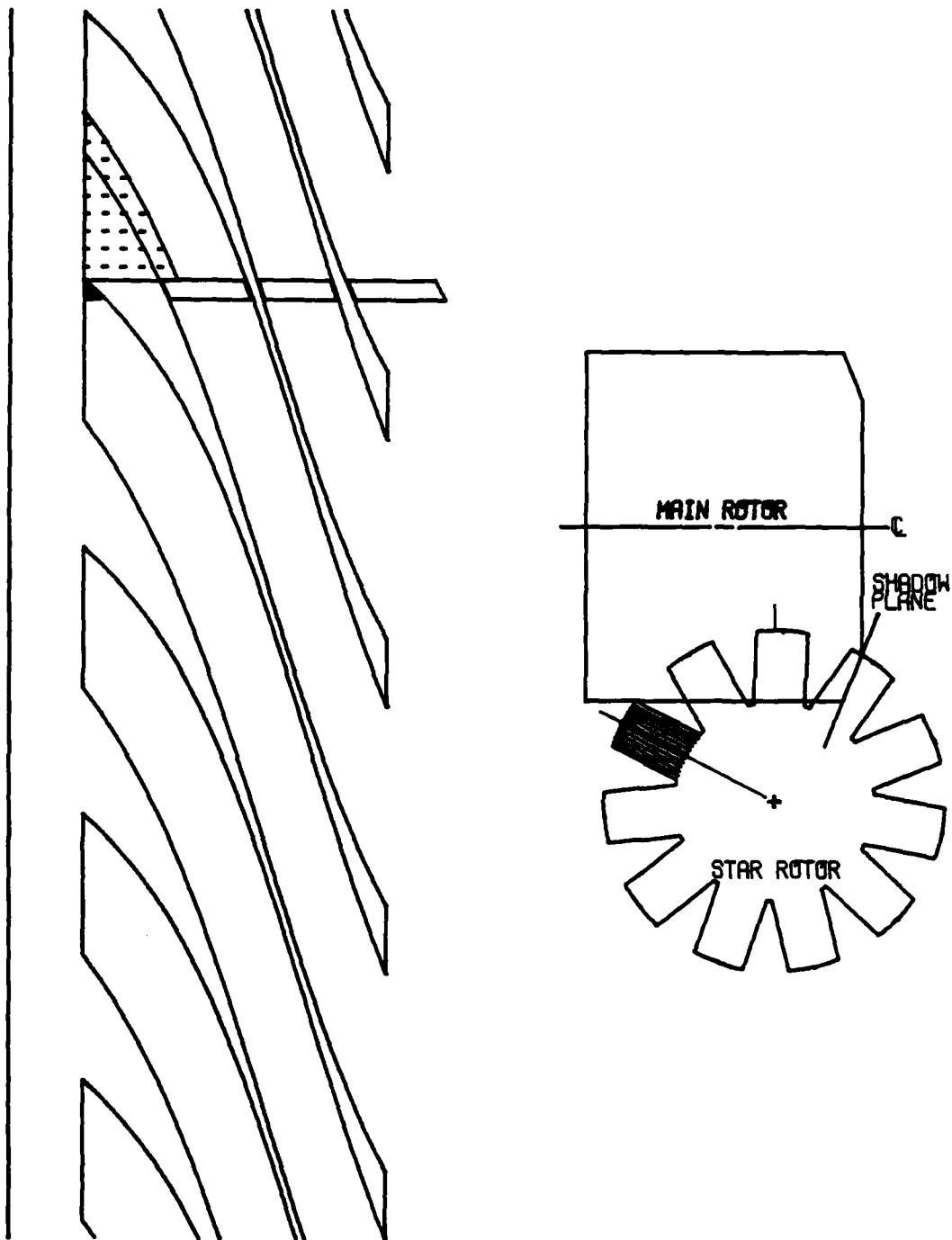Figure 20.
Beginning of Discharge Process

Figure 21.
End of Discharge Process

T_p = The predicted temperature.

Having compressed the air, the control volume boundary is conceptually opened allowing flow through the discharge port. Returning to the first law of thermodynamics, the relationship is written:

$$\delta Q - \delta W + h_{in} dm_{in} - h_{out} dm_{out} = dU_{cv} \tag{1}$$

First, discussing flow into the control volume, this is rewritten assuming zero heat transfer during flow through the port, zero work done, and zero flow out of the control volume:

$$h_{in} dm_{in} = dU_{cv}$$

Recognizing that the air flowing into the control volume is at the discharge plenum conditions which are constant by assumption, $h_{in} = h_{disch}$. Integrating this becomes:

$$h_{disch} m_{in} = m_{n+1} u_{n+1} - m_n u_p$$

Where:

h_{disch} = Specific enthalpy of air in the discharge plenum.

m_{in} = Mass of air that crossed control volume boundary during the increment.

m_{n+1} = Total mass of air in control volume at the end of increment.

U_{n+1} = Specific internal energy of air at the end of increment.

U_p = Specific internal energy of air at predicted conditions.

The pressure gradient across the discharge port is the average of the predicted and initial pressures. The mass of air that flows through the discharge port is evaluated using the average pressure gradient and a constant air density evaluated at the conditions of the discharge plenum. The mass flow of oil is also evaluated using the average pressure in the control volume. Relating specific enthalpy in terms of specific heat at constant volume, the corrected temperature is evaluated by:

$$T_c = \frac{h_{disch} m_{in} + m_n U_p}{m_{n+1} \, c_v}$$

The corrected pressure is then found by the ideal gas relationship using:

$$P_c = \frac{(m_n + m_{in}) \, R \, T_c}{V_{n+1}}$$

If the predicted and corrected pressures are not within a tolerance limit the pressure gradient is set to be the average of the corrected pressure and the initial pressure. The flow relations are then reevaluated until the limit is satisfied.

For the second case, where the flow is out of the control volume, the energy relationship becomes:

$$-h_{out} dm_{out} = dU_{cv}$$

Integration of this relationship is not straightforward because the properties of the air leaving the control volume vary. By convention dm_{out} will be negative. Recognizing that $dm_{out} = dm_{cv}$ and writing in terms of specific heats:

$$c_p T_{out} dm_{cv} = c_v (m_{cv} dT_{cv} + T_{cv} dm_{cv})$$

But $T_{out} = T_{cv}$, simplifying:

$$\frac{(c_p - c_v)}{c_v} \frac{dm_{cv}}{m_{cv}} = \frac{dT}{T_{cv}}$$

Integrating and simplifying:

$$\frac{T_2}{T_1} = \left[\frac{m_2}{m_1}\right]^{k-1}$$

Where:

T_1 = Temperature in control volume before flow

T_2 = Temperature in control volume after flow

m_1 = Mass in control volume before flow

m_2 = Mass in control volume after flow

This can be rewritten in terms of P and m by the ideal gas relation as:

$$\frac{P_2}{P_1} = \left[\frac{m_2}{m_1}\right]^{k}$$

Rewritting in terms of P_c, P_p and increment notation:

$$P_c = P_p (m_{n+1}/m_n)^k$$

The mass flow of air is evaluated by Bernoulli's equation as described for equation (4). The mass flow of air is dependent on the density and pressure in the control volume and the mass flow of oil is dependent on the pressure in the control volume. Therefore, average values of pressure and density will be used in the computations.

The temperature at the end of the increment is found from the ideal gas relation:

$$T_{n+1} = \frac{P_{n+1} V_{n+1}}{m_{n+1} R}$$

The case when P_c is less than the discharge pressure is physically unrealistic and can be corrected in a few ways. These are to take smaller increment steps, to assume that P_c will be equal to the discharge pressure at the end of the time step, or, to adjust the predicted pressure so that the pressure at the end of the increment is the discharge pressure. The last alternative was chosen because with it, a pressure gradient across the discharge port is calculated. This is not only used to evaluate the mass of air that leaves the control volume, but it is needed to evaluate the mass of oil that leaves the control volume. With this approach, the mass of air and mass of oil can be tracked during the discharge process.

For this case when P_c is less than the discharge

pressure, the total volume of the air and oil in the control volume is compared to the volume of the control volume. If the difference between these volumes is more than a tolerance limit the predicted pressure is adjusted using the secant method for interpolation. The procedure is repeated until the difference between the volume of the air and oil, and the volume of the control volume, are within the limit set. This procedure is conceptually presented, Figure 22, on pressure versus volume coordinates for 2 iterations.

Figure 22.
Predictor Corrector Scheme for the
Discharge Process

LEAKAGE PATHS

DEFINITION

From the original set of assumptions, only oil will be considered to pass through the leakage paths that are on the boundary of the control volume. It will also be assumed, that only air will pass through the inlet port. For the discharge port, when the pressure within the control volume is lower than the discharge plenum pressure, only air will be assumed to flow from the discharge plenum into the control volume. Conversely, when the pressure in the control volume is greater than the discharge plenum pressure, both air and oil will be considered to flow out of the control volume. For this case, the oil and air will be considered as individual fluids, each passing through a proportion of the open discharge port. The proportion will be determined by the ratio of their respective volume to the available thread volume at the increment being evaluated.

There are 9 leakage paths through which fluid can flow either into or out of the control volume. These are:

1.) Star rotor tip

2.)   Star rotor leading flank

3.)   Star rotor leading flank blowhole

4.)   Star rotor trailing flank

5.)   Star rotor trailing flank blowhole

6.)   Star rotor window

7.)   Main rotor leading thread land

8.)   Main rotor trailing thread land

9.)   Main rotor discharge end band

These paths are identified on Figure 23 and on Figure 24. For the analysis of these paths, they will be divided into three categories and each category will then be developed. The categories are as follows with the applicable leakage paths also listed:

I.   Constant Clearance Gap

    a)   Star rotor window

    b)   Main rotor leading thread land

    c)   Main rotor trailing thread land

    d)   Main rotor discharge end band

II.   Variable Clearance Gap

    a)   Star rotor tip

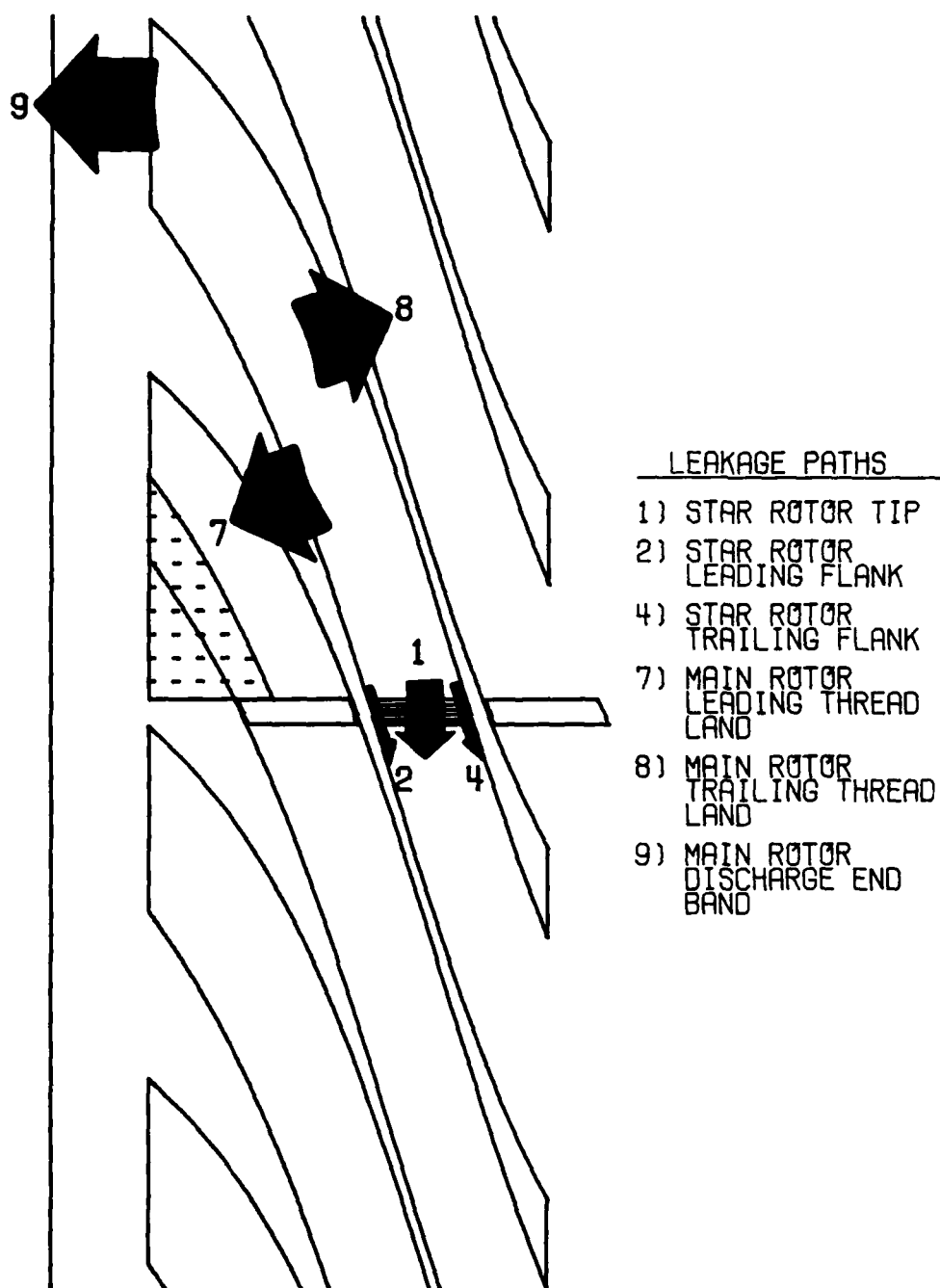   b)   Star rotor leading flank
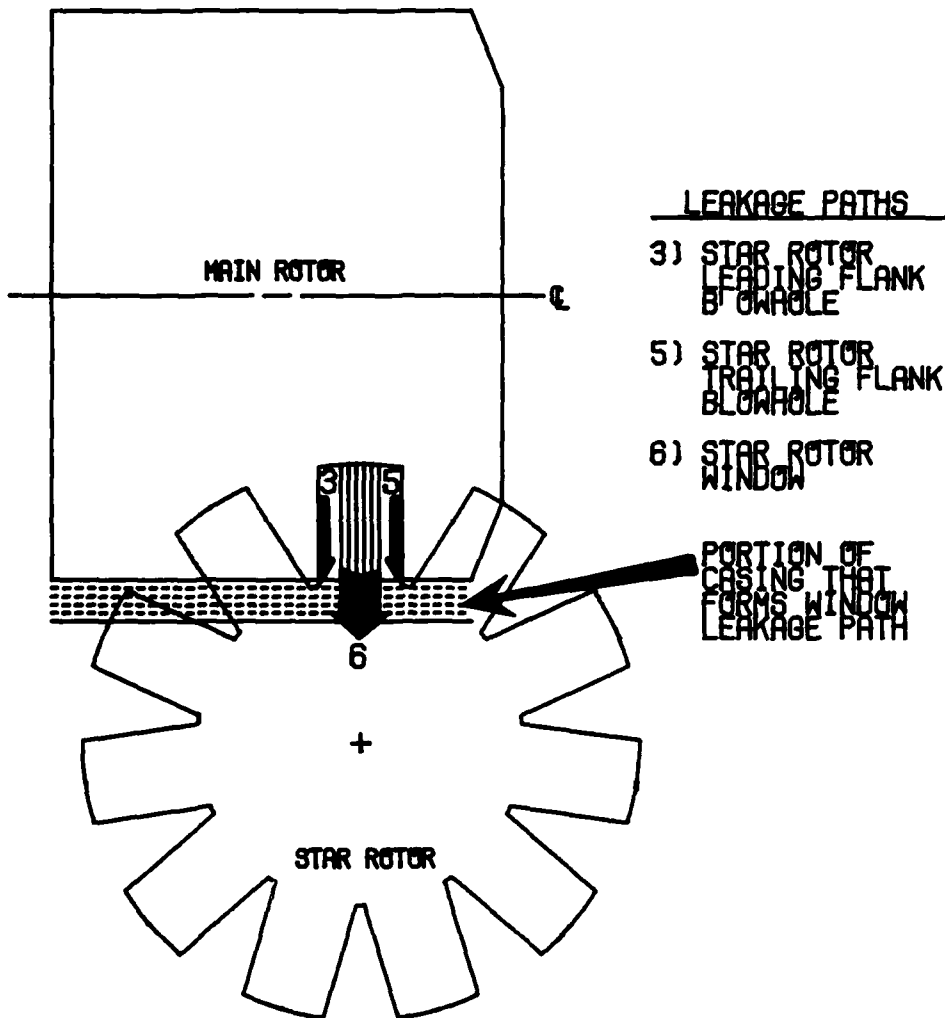
Figure 23.
Leakage Paths - Main Rotor View

LEAKAGE PATHS

3) STAR ROTOR
LEADING FLANK
BLOWHOLE

5) STAR ROTOR
TRAILING FLANK
BLOWHOLE

6) STAR ROTOR
WINDOW

PORTION OF
CASING THAT
FORMS WINDOW
LEAKAGE PATH

MAIN ROTOR

STAR ROTOR

Figure 24.
Leakage Paths - Star Rotor View

  c)   Star rotor trailing flank

III. Orifice Type

  a)   Star rotor leading flank blowhole

  b)   Star rotor trailing flank blowhole

The assumption of – only oil is present at the leakage paths – will have a significant effect on the results of this model. It is based on the premise that the oil is directed to the leakage paths by the rotating motion of the components. Oil that is attached to the main rotor will tend to be forced toward the outside of the main rotor by the centrifugal effects resulting from the rotating main rotor. This will serve to direct oil to the leading thread land, trailing thread land and discharge end band leakage paths. By the same reasoning, oil will tend to be forced toward the tip of the star rotor. As the star rotor progresses through the thread in the main rotor, it will "wipe off" the oil attached to the main rotor. The oil that is "wiped off" by the main rotor will then tend to collect at the location where the main rotor thread and star rotor flank come together. By this reasoning, oil will then tend to collect at the star rotor leading flank, star rotor leading flank blowhole, star rotor trailing flank and star rotor trailing flank blowhole leakage paths. The only leakage path not accounted for by these arguments is the star rotor window path. But, the window leakage path will be covered

with oil when enough oil is "wiped off" the main rotor by the star rotor flanks and tip and collects on the surface of the star tooth. It is recognized that in the early part of the compression cycle, this reasoning suggests that air may be passing through the window leakage path. But, the pressure in the control volume is low in the beginning of the cycle and it is felt that the error introduced will not be significant. The assumption that only oil is present at the leakage paths will be tested by whether or not the model predicts changes for which operating data is available.

Flow paths that have very short throttling lengths will be considered to be orifices. The criteria for this will be $(L/D) < 2.5$; where L is the throttling length parallel to the flow and D is the hydraulic diameter. [5] Where the hydraulic diameter is expressed by the following relation:

$$D = 4(\frac{\text{cross sectional flow area}}{\text{wetted perimeter}})$$

For small clearances and wide paths, such as those encountered in the single screw compressor, the hydraulic diameter is approximately 2 times the clearance. The governing equation for flow through the orifice paths will be Bernoulli's equation previously developed.

The governing equation for incompressible flow not considered to be orifice flow will be Darcy's formula. This is:

$$h_L = \frac{\Delta P}{\rho} = \frac{V^2}{2} \, f \, \frac{L}{D} = K \, \frac{V^2}{2}$$

Where:

f = friction factor.

h_L = head loss across path.

K = resistance coefficient.

ΔP = pressure drop across path.

V = velocity of flow through path.

ρ = mass density of flowing fluid.

The losses of a fluid flowing through a particular path are generally a result of viscous effects and a result of changes in speed and direction of the flow path. To adjust the predicted flow rate to match the flow rate obtained from operating data, correction factors are typically used. For this study the correction factors will only "tune" the non-viscous losses. The viscous losses are quite well defined, especially in the laminar flow region, and will not be considered to be effected by the speed at which the parts are moving relative to each other. The non-viscous effects will, however, be effected by the speed of the parts. It is recognized that the correction factor that will be used will be an average value. The relative speed between the parts will change during the cycle. By using an average correction factor, the error in the calculated oil flow through the particular path will have a negligible effect on the predicted pressure history in the control volume.

CONSTANT CLEARANCE GAP

This type of leakage path is commonly described as flow between parallel plates, Figure 25. To be applicable to all of the single screw compressor leakage paths that are of this type, the equations that will be developed will include the Poiseuille flow, the Couette flow, the non-viscous effects and a correction factor. In addition, a technique will be developed that will be able to accommodate a throttling length that is not the same from one side of the leakage path to the other, Figure 26.

The Poiseuille flow will be evaluated using Darcy's equation. From experience, it has been found that the flow is laminar through this type of leakage path when the flowing fluid is oil. Stepanoff [6] presents data for flow through annular gaps. This is a close approximation to flow through a rectangular path. From the presented data, the following approximation will be used for the friction factor:
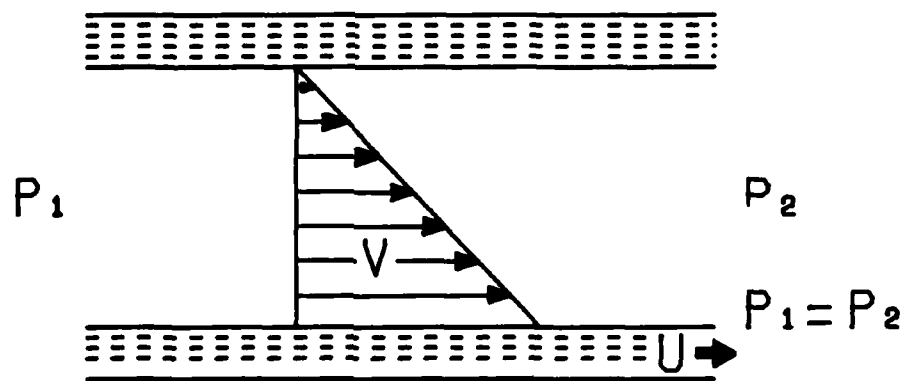
$$f = \frac{64}{R_e} = 64 \frac{\nu}{VD}$$

Where:

R_e = Reynolds number

ν = Kinematic viscosity of flowing fluid

The non-viscous losses will be lumped as entrance and exit losses, with sharp-edged entrance and exit assumed.
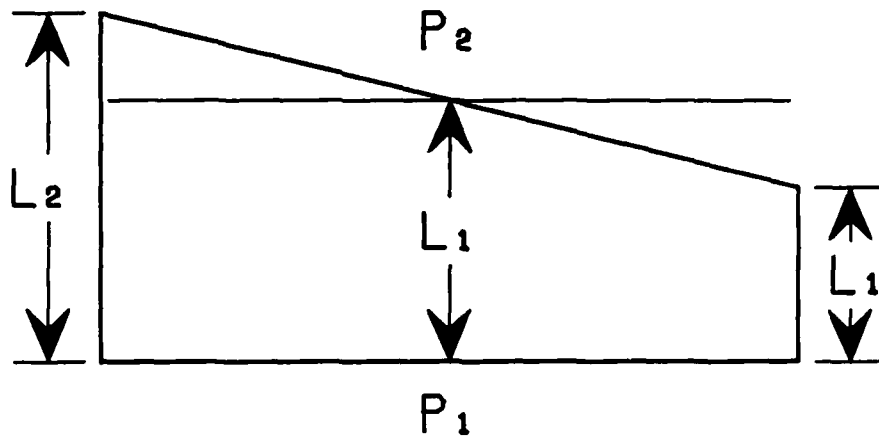
POISEUILLE FLOW

COUETTE FLOW

Figure 25.
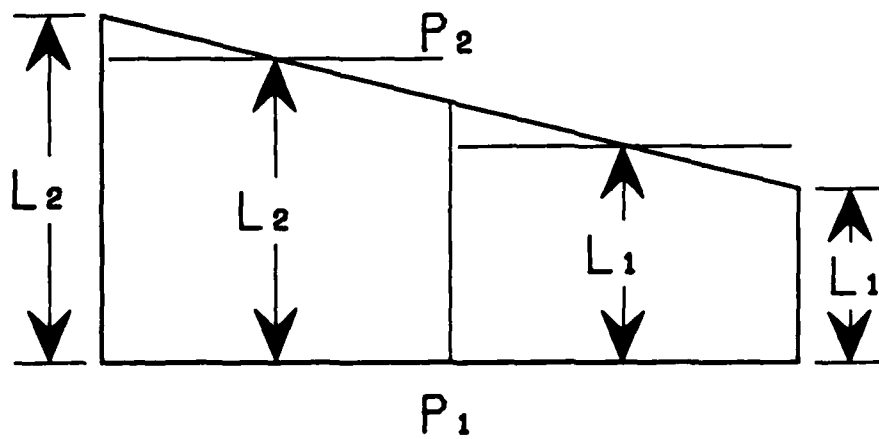Poiseuille and Couette Flow Patterns

$P_1 > P_2$

Figure 26.
Plan View of Unequal Throttling Length Path

Combining the viscous and non-viscous contributors to the head loss and introducing F as the correction factor, the resulting relation is:

$$\frac{\Delta P}{\rho} = F\ 1.5\ \frac{V^2}{2} + 64\ \frac{\nu}{V\ D}\ \frac{L}{D}\ \frac{V^2}{2} \tag{5}$$

Simplifying, the equation can be written:

$$V^2(F\ 0.75) + \frac{32\ L\ V\ \nu}{D^2} - \frac{\Delta P}{\rho} = 0$$

This can readily be solved with the quadratic formula for V.

Combining the Poiseuille and Couette components, the total mass flowrate through the leakage path is then given by:

$$\dot{m} = (V + \frac{U}{2})\ \text{AREA}\ \rho$$

Where:

$\dot{m}$ = Mass rate of flow through the leakage path.

U   = Velocity of the moving plate.

AREA = Cross sectional area of leakage path.

The non-viscous losses have a greater effect on the velocity of the flow through the path for short throttling lengths than for long throttling lengths. The technique for evaluating the leakage through a path with unequal throttling lengths accounts for this difference in the following way. The flowrate is first computed with an average of L_1 and L_2, denoted as L' on Figure 26. The width of the leak-

age path, w, is cut in half and the total flowrate is the sum of the flow from the half with L_1', as the throttling length and the flow from the half with L_2' as the throttling length. This total flowrate is then compared to the previous total flowrate. If the difference between the two is above a tolerance limit, the width is divided into progressively more pieces until the limit is satisfied. This then can be thought of as an integration across the width of the leakage path that accounts for the non-linear effect of the non-viscous losses.

VARIABLE CLEARANCE GAP

For this type of leakage, the standard Darcy equation cannot be employed directly because the clearance between the two plates changes in the direction of the flow, Figure 27. The relationship for the Couette flow will still be considered valid as will the approach applying a general correction factor to the non-viscous losses. In order to get a representation of the flow due to the viscous effect, attention is focused on the resistance coefficient from Darcy's equation. Writing the change in throttling length as ΔL, and separating the empirical resistance coefficient values for the entrance and exit losses this becomes:

$$\Delta\frac{P}{\rho} = (0.5)\ \frac{v^2_{ent}}{2} + (1.0)\ \frac{v^2_{exit}}{2} + f\ \left(\frac{L}{D}\right)\ \frac{v^2}{2} \qquad (6)$$
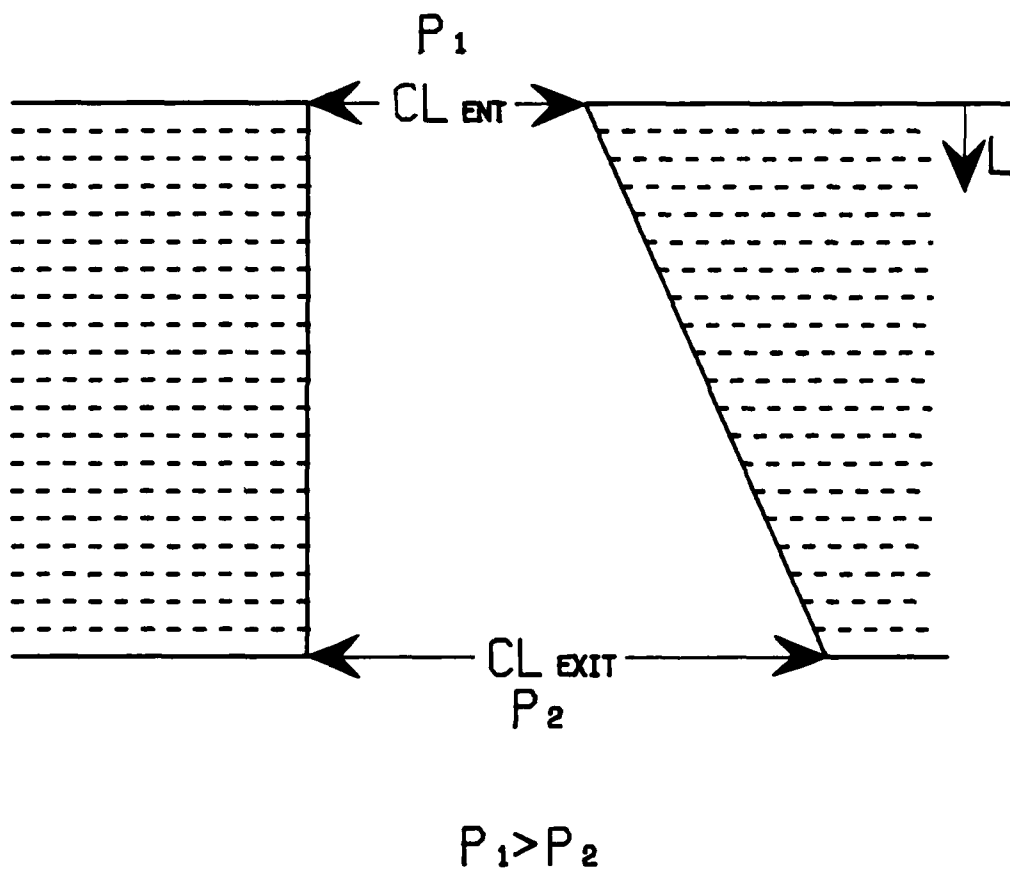
Where:

Figure 27.
Divergent Leakage Path

V_{ent} = Velocity through the clearance on high pressure side.

V_{exit} = Velocity through the clearance on low pressure side.

Again, the flow in this case is laminar, so the friction coefficient is replaced with $64/R_e$. Also, the velocity through the gap will change as the fluid moves through the gap according to the clearance between the plates. But, by continuity, the volumetric flowrate through the gap will remain constant at different points through the gap. Therefore, V will be replaced with:

$$V = \frac{\dot{Q}}{w_{cl}}$$

Where:

cl = Clearance between plates.

$\dot{Q}$ = Volumetric flowrate.

w = Width of gap.

Substituting for V, using subscripts to indicate entrance and exit clearances, replacing the hydraulic diameter with twice the clearance between the plates and simplifying, equation (6) becomes:

$$\Delta \frac{P}{\rho} = \frac{\dot{Q}^2}{4\ w^2\ cl^2_{ent}} + \frac{\dot{Q}^2}{2\ w^2\ cl^2_{exit}} + \frac{8\ \nu\ \Delta L\ \dot{Q}}{w\ cl^3}$$

Taking the limit as $\Delta L \rightarrow 0$ and integrating:

$$\Delta\frac{P}{\rho} = \frac{\dot{Q}^2}{w^2}\left[\frac{1}{4\ cl^2_{ent}} + \frac{1}{2\ cl^2_{exit}}\right] + \frac{8\ \nu\ \dot{Q}}{w}\int_{L=0}^{L=L}\frac{dL}{cl^3}$$

Conveniently, the clearance between the plates can be expressed in terms of the throttling length by:

$$cl = a + b\ L$$

Where:

a = Clearance at L=0.

b = Slope of angled plate.

Substituting, carrying out the integration, and simplifying:

$$\frac{\Delta P}{\rho} = \frac{F\ \dot{Q}^2}{w^2}\left[\frac{1}{4\ cl^2_{ent}} + \frac{1}{2\ cl^2_{exit}}\right] + \frac{8\ \nu\ \dot{Q}}{w}\frac{1}{2b}\left[\frac{1}{a^2} - \frac{1}{(a+b\ L)^2}\right]$$

(7)

This relationship can be solved for $\dot{Q}$ by using the quadratic equation. The total mass flowrate through the gap is now written as:

$$\dot{m} = \dot{Q}\ \rho + \frac{U}{2}\ w\ cl \tag{8}$$

This same technique of integrating for the viscous resistance coefficient is used for leakage paths that have a change in the variable clearance gap. As an example, Figure 28 is a convergent divergent flow path. By treating the two sections separately, the total resistance to flow will have
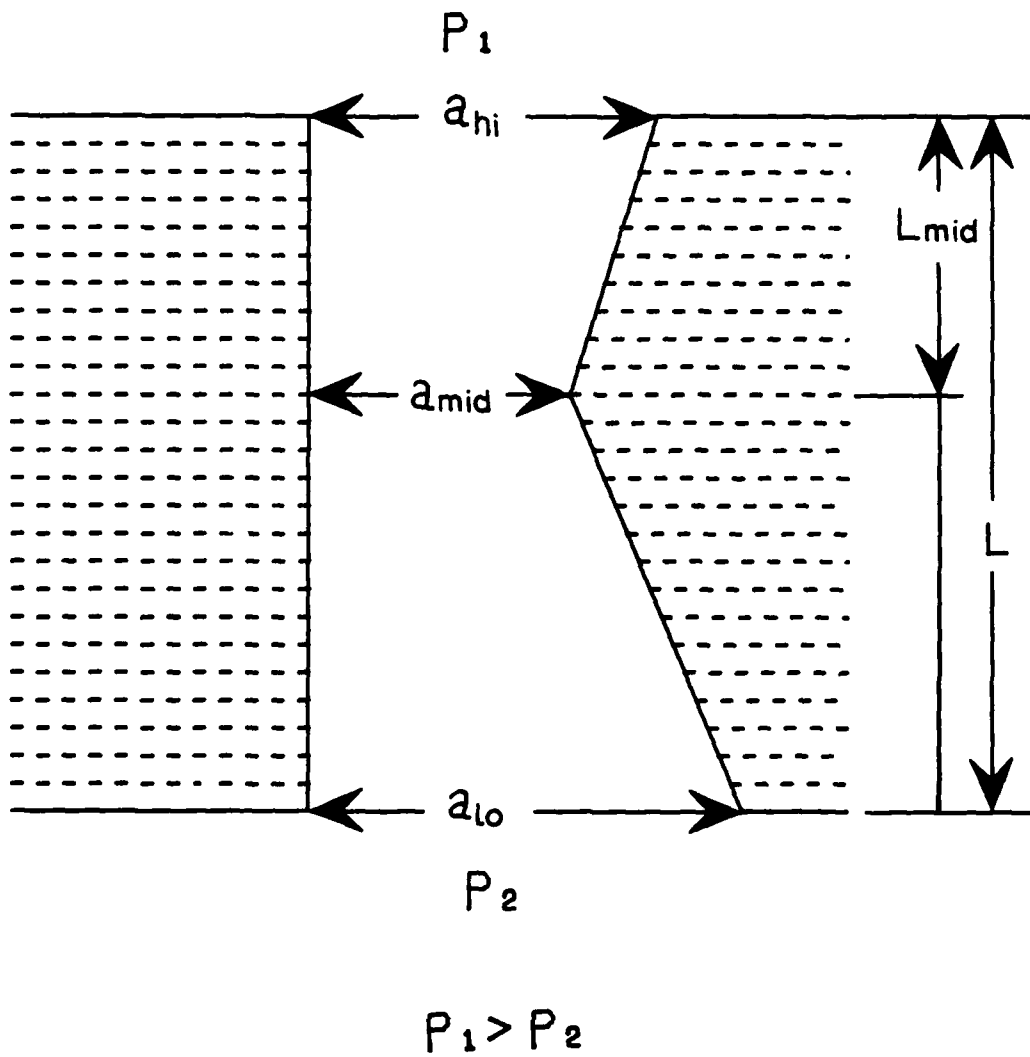
Figure 28.
Convergent Divergent Leakage Path

the non-viscous losses, the convergent section loss and the divergent section loss. The integration for the viscous losses will, therefore, be performed for the appropriate length. Writing just the integrated viscous term for the convergent section, it is:

$$\frac{8 \, \nu \, \dot{Q}}{w \, 2 \, b_{hi}} \left[\frac{1}{a_{hi}^2} - \frac{1}{(a_{hi} + b_{hi} \, L_{mid})^2} \right]$$

Where:

a_{hi} = Clearance at L=0.

b_{hi} = Slope of convergent plate.

L_{mid} = Throttling length to where divergent path begins.

Similarly for the divergent section:

$$\frac{8 \, \nu \, \dot{Q}}{w \, 2 \, b_{lo}} \left[\frac{1}{a_{mid}^2} - \frac{1}{(a_{mid} + b_{lo} \, (L - L_{mid}) \,)^2} \right]$$

Where:

a_{mid} = Clearance at $L=L_{mid}$.

b_{lo} = Slope of divergent plate.

When these contributions are substituted into equation (7), the relation can again be solved for $\dot{Q}$. The total mass flowrate through the gap is the same as equation (8).

DISCHARGE PORT

There is a leakage path at the discharge port that is not within the control volumes previously defined. Figure

29 shows the direction and location of the flow. The fluid leaking through this path will be assumed to be air. This is consistent with the assumption that there will not be any backflow of oil into the control volume from the discharge plenum. The flow will be assumed to be one dimensional and isentropic. The governing equation used is derived by Soedel in [7], and the result is written as:

$$\dot{m} = A \ P_{DP} \ \sqrt{\frac{2 \ k}{(k-1) \ R \ T_{DP}}} \ \sqrt{r^{\frac{2}{k}} - r^{\frac{k+1}{k}}} \qquad (9)$$

Where:

   A   = Cross sectional area.

   P_{DP} = Pressure, discharge plenum.

   T_{DP} = Temperature, discharge plenum.

   r   = Pressure ratio.

It should be noted that r is limited by the critical pressure ratio. This is written:

$$\frac{P_{DP}}{P_{lo}} < r_c \qquad r = \frac{P_{DP}}{P_{lo}}$$

$$\frac{P_{DP}}{P_{lo}} > r_c \qquad r = (\frac{2}{k+1})^{\frac{k}{k+1}}$$

Where:

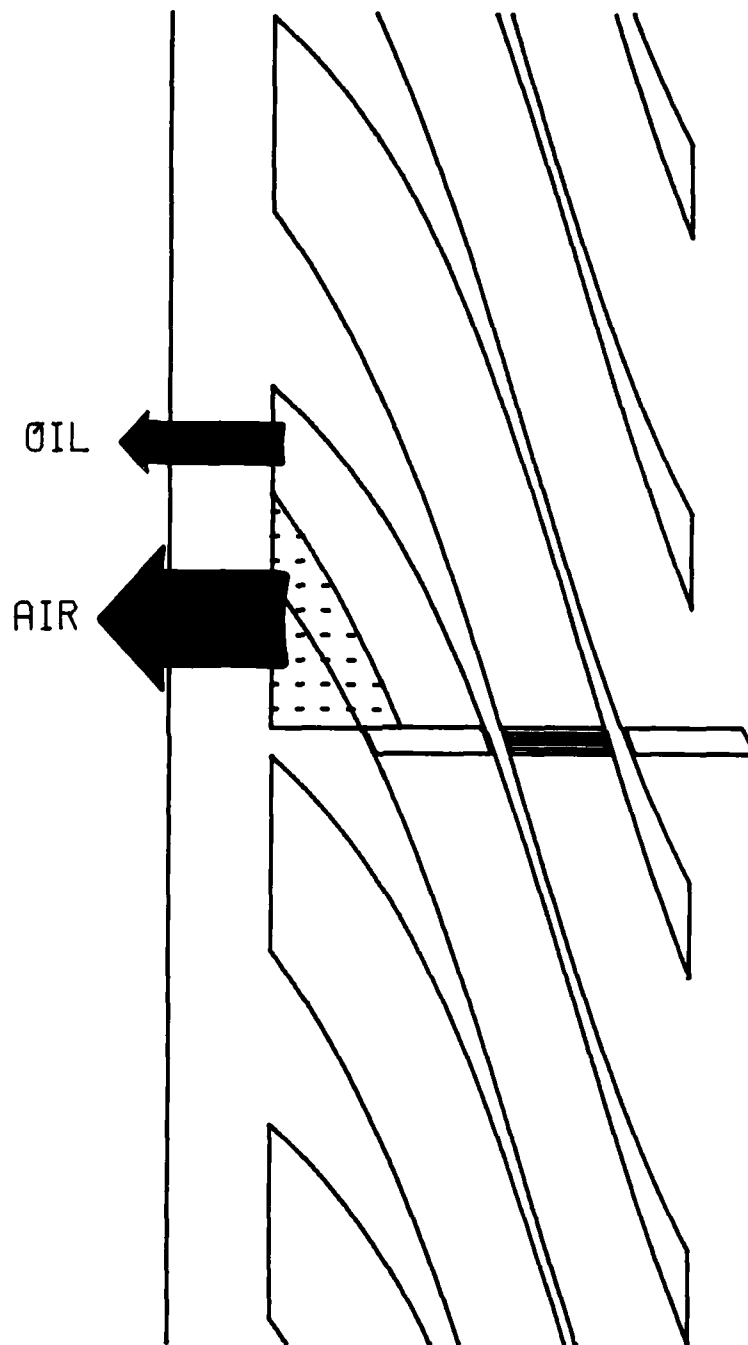 P_{lo} = The downstream pressure.

Figure 29.
Discharge Port Leakage Path

r_c = Critical pressure ratio.

The assumption that air is leaking through the path, does not account for the fluid in the path. Referring to Figure 29, and ignoring the other threads for a moment, it can be seen that oil flows between the main rotor and housing before the thread reaches the discharge port. Having reached the discharge port, air flows between the housing and the main rotor. But before the air can flow through the gap, according to the governing equation, the oil must be pushed out of the gap. As a result of this argument, a correction factor will be applied to equation (9). This correction factor will be determined by correlating the predicted values with the available empirical values.

ADJUSTMENT OF CORRECTION FACTORS WITH EMPIRICAL DATA

The empirical data that was used in the computer model
was obtained by tests performed at the David W. Taylor Naval
Ship Research and Development Center, Code 2722, Annapolis,
Maryland. The following empirical values are used in the
model:

1. Suction air temperature.

2. Oil injection temperature.

3. Air-oil mixture discharge temperature.

4. Suction pressure.

5. Discharge pressure.

6. Diameter, flow coefficient, pressure and location of
    oil injection port.

7. Pressure in area in front of discharge end of main
    rotor.

Empirical data is used to determine the effect the suc-
tion air preheat has on the volumetric efficiency of the
compressor. The flowrate of air through the compressor is
dependent on the mass of air that fills the main rotor
thread before beginning the compression cycle. In this
case, the mass of air is dependent on the temperature of air
that fills the thread. Heat is transferred to the air from
the intake piping and from the injection oil. In Figure 30,
the effect inlet air temperature has on the volumetric

efficiency of the compressor is shown. The curve is a least squares fit of data taken at a discharge pressure of 930 KPa, and an oil injection temperature of 60 C. An empirical relationship was developed to predict the average temperature of the air that fills the main rotor thread.

$$T_{CVI} = T_i \left(1 + \alpha \left(\frac{T_{oil}}{T_i} - 1\right)\right)$$

Where:

T_{CVI} = Air temperature in thread before beginning compression, control volume I.

T_i = Air temperature entering inlet filter.

T_{oil} = Oil injection temperature.

α = Inlet heat transfer coefficient.

The value of α was evaluated to be 0.52 for this compressor at the stated conditions. It should be noted that the value of α will be a function of oil injection temperature, inlet passage geometry, flowrate through the compressor and the leakage characteristics of the compressor.

Empirical data is also necessary to evaluate the effect of leakage from the control volumes. Beginning with the star tip, tests had been performed with the only variable being the clearance at the tip of the star rotor. These tests were made by progressively machining the outside
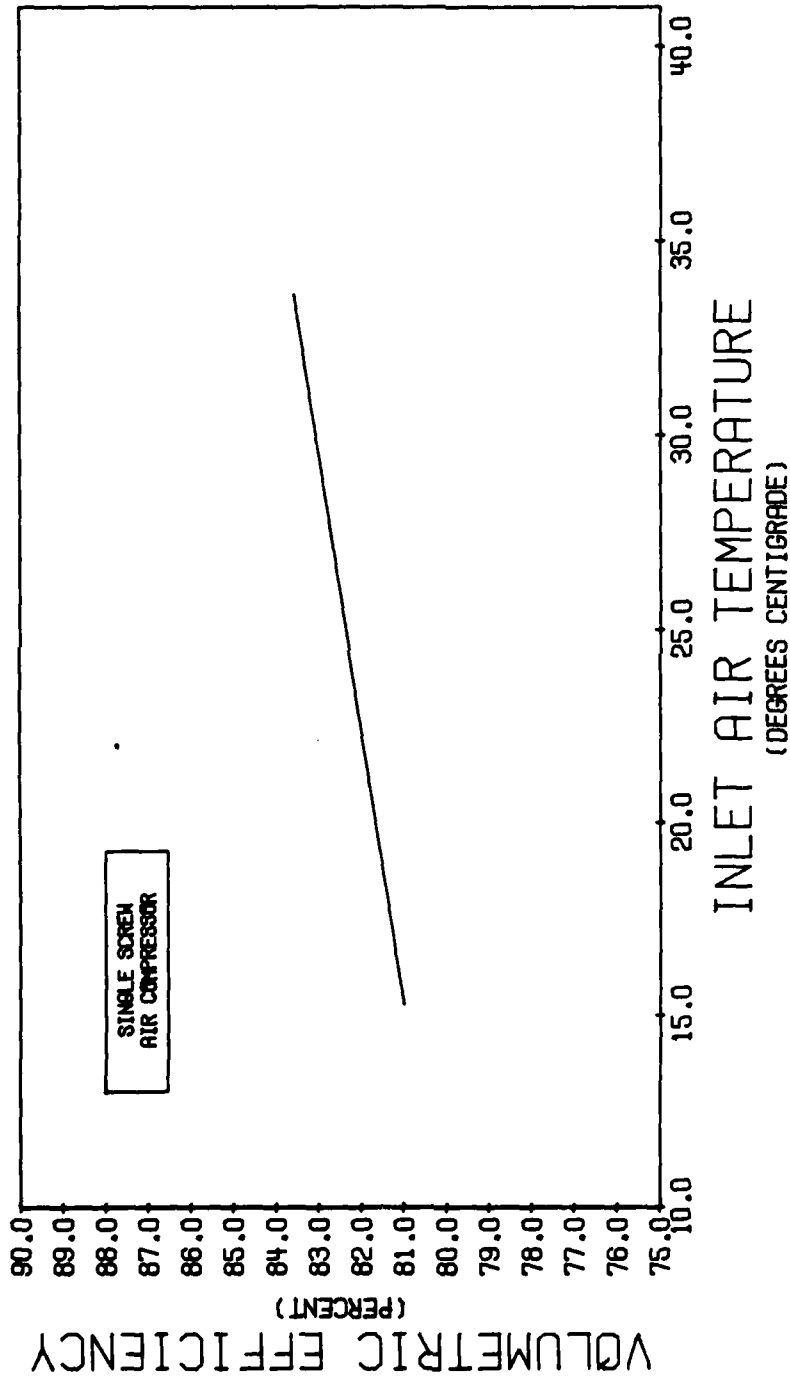
Figure 30.
Volumetric Efficiency as a Function of
Inlet Air Temperature

diameter of the star rotor.In Figure 31,the volumetric effi-
ciency is shown for 0.010, 0.020, and 0.030 centimeters off
of the original outside diameter of a pair of star rotors.
The values shown are corrected to an inlet air temperature
of 24 C.

In the development of the leakage paths from the con-
trol volumes, correction factors were introduced that
effected only the non-viscous losses. The star rotor tip
correction factor was adjusted at a discharge pressure of
965 KPa, until the change in volumetric efficiency, due to
the respective change in star rotor tip clearance, approxi-
mated the change measured in the empirical data. Using an
initial star rotor tip clearance of 0.018 cm, the star rotor
correction factor was evaluated to be 0.05. This low value
indicates that the head loss through the star rotor tip path
is primarily due to the viscous effects.

In Figure 32, the change in volumetric efficiency
between two star tip clearances is shown. The empirical
value and the computer model value are shown side by side.
The change in volumetric efficiency is used because the
absolute values are not know, only the change in overall
volumetric efficiency for a change in clearance is known.

Empirical data is not available for changes in star
rotor flank clearance. The correction factor determined for
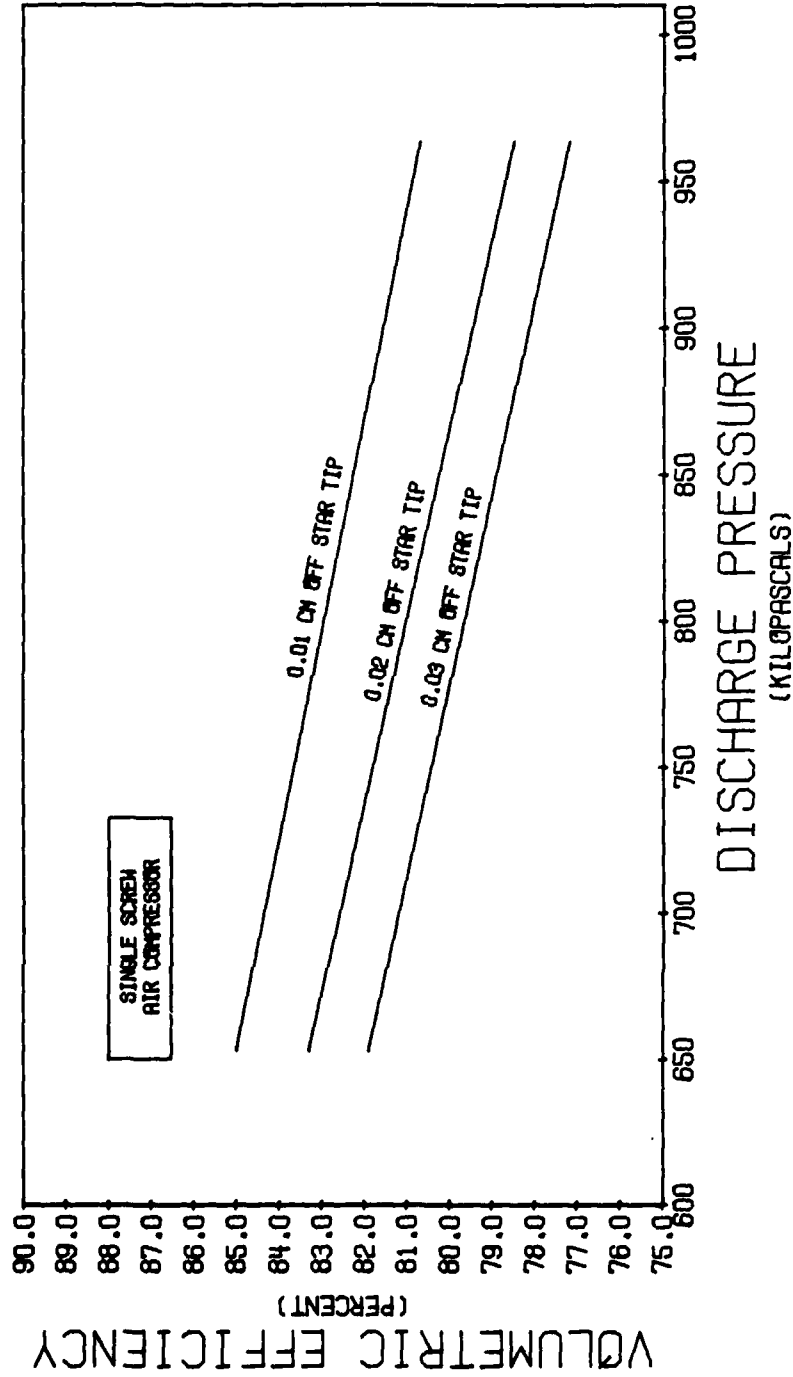the star rotor tip will also be used as the correction

Figure 31.
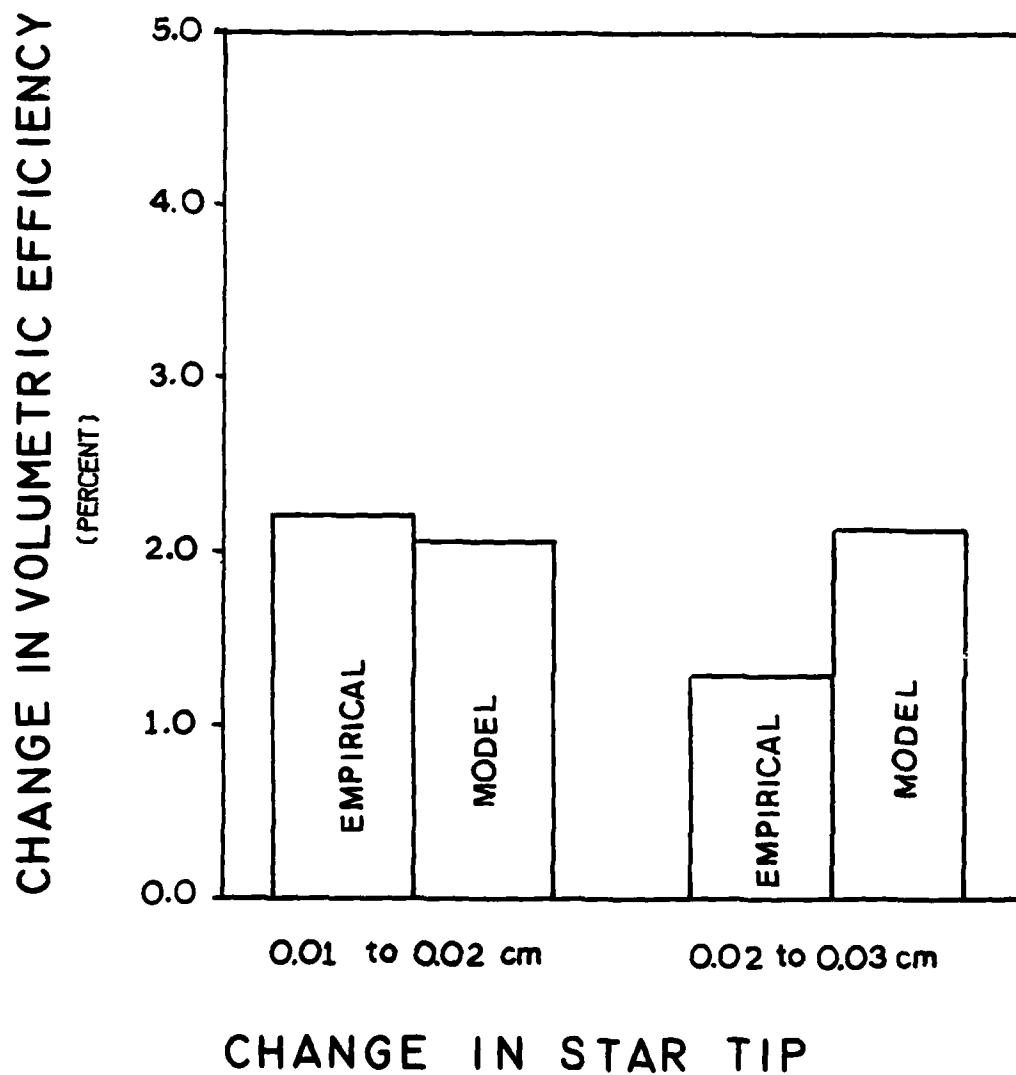Volumetric Efficiency for Changes in Star
Tip Clearance - Empirical

Figure 32.
Change in Volumetric Efficiency for Changes
in Star Tip Clearance

factor for the star rotor flanks. This decision is based on the similarity of the star rotor tip and star rotor flank leakage paths. In addition, it is theorized that the non-viscous losses are primarily a function of the difference of the moving wall speed, relative to the leakage path, and the poiseuille flow average velocity. If this theory is correct, then using the tip correction factor for the flank leakage path will produce conservative predictions for flank losses. This is because the moving wall speed relative to the flank is higher than the moving wall speed relative to the tip.

Empirical data is available for changes in the star rotor window clearance. This data is similar to that described for the star rotor tip in that tests were conducted for a series of star rotor window clearances. In Figure 33, the volumetric efficience with a window clearance of 0.013, 0.023, and 0.033 cm is shown. The values were obtained with all other clearances back to the normal values, and are corrected to an inlet temperature of 24 C.

The correction factor for the star window was adjusted at a discharge pressure of 965 KPa until the change in volumetric efficiency, due to the respective change in star window clearance, produced the best approximation to the change measured in the empirical data. The correction factor for the star window was evaluated to be 0.02. This is close to the value of the star tip correction factor. It
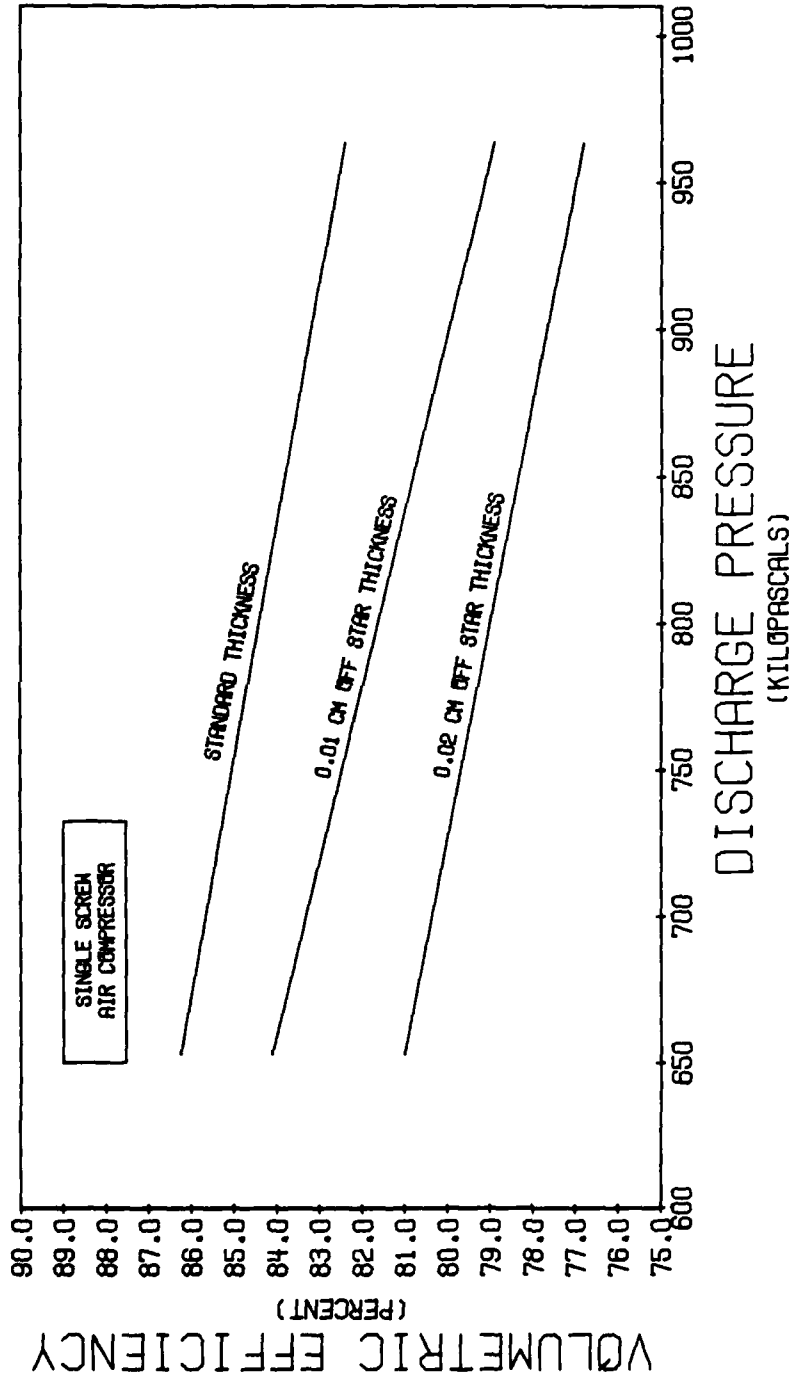
Figure 33.
Volumetric Efficiency for Changes in the
Window Clearance – Empirical

should be noted that these correction factors are an average factor for the entire compression cycle.

In Figure 34, the change in volumetric efficiency between two star window clearances is shown. The empirical value and the computer model value are shown side by side. There is no empirical data available to set correction factors on the non-viscous losses for the main rotor leading thread and trailing thread lands. The relationship between the poiseuille flow velocity and the speed that the land is moving was compared to the same values evaluated at the star rotor tip. As a result, an average value for the correction factor for the main rotor leading thread and trailing thread land of 0.10 will be used.

The final correction factor that is used is the one associated with the discharge port leakage path. For this path, the leaking fluid is air, but, oil also leaks through the same path. The correction factor will adjust the maximum possible air flow to the amount of air that can flow after the oil is pushed out of the leakage path.

The predicted volumetric efficiency of the compressor is more sensitive to the choice of the correction factor for the discharge port leakage path than for any of the correction factors previously discussed. By evaluating the volumetric efficiency predicted by the model for maximum and minimum correction factor for each of the other paths, the

‖‖ 1.0

2.8   ‖ 2.5

‖ 2.2

‖ 2.0

‖‖ 1.1

‖ 1.8

‖‖ 1.25   ‖ 1.4   ‖ 1.6
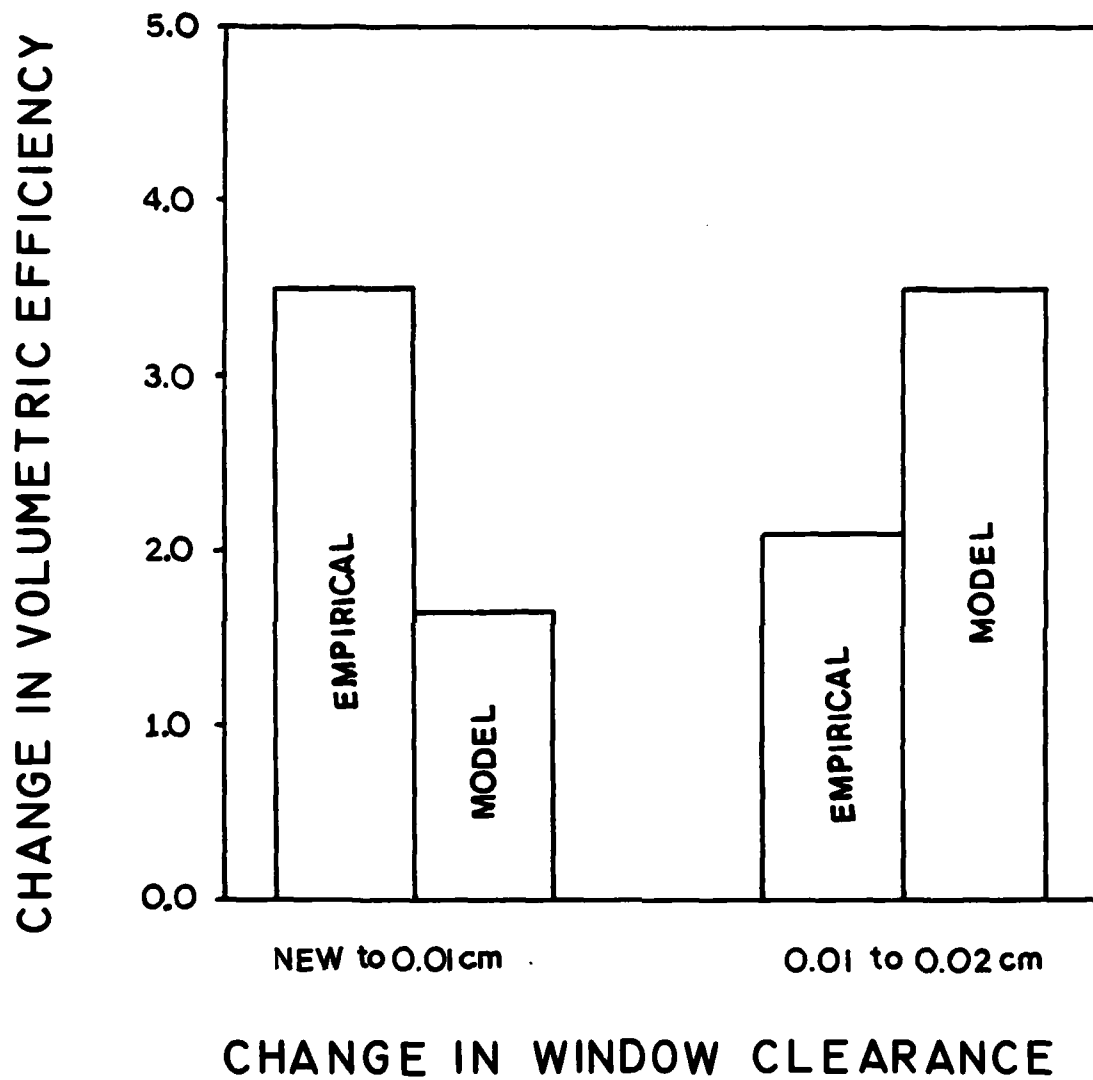
MICROCOPY RESOLUTION TEST CHART

Figure 34.
Change in Volumetric Efficiency for Changes
in the Window Clearance

largest change in volumetric efficiency, at standard clearance, was about 5%. By contrast, varying the correction factor from maximum to minimum, for the discharge port leakage path, changes the volumetric efficiency by more than 50% at 965 KPa discharge pressure. There are two factors causing this large difference. First, the previous correction factors only effect the non-viscous losses, whereas, the correction factor for the discharge port leakage path adjust the maximum possible flow. Second, the previous correction factors were leakage paths where oil was the flowing fluid. In this case, the fluid is air, so the higher flowrate is not unexpected.

Although the available empirical data does not evaluate changes in the clearance of the discharge gap, the data available is sufficient to evaluate what value to assign to the discharge port correction factor. The effect on the volumetric efficiency due to the suction air preheat and the various leakage paths have each been tuned in the model to yield the response measured by the empirical data. The only leakage path unaccounted for is the effect due to the discharge port leakage. Therefore, the discharge port leakage path correction factor will be adjusted until the model predicts the same value as the empirical data at a particular point. The factor was evaluated to be 0.154, using a discharge pressure of 965 KPa as the comparison point. An interpretation of this value is that for approximately 85%

of the time, the air flow through the discharge port leakage
path is blocked by oil.

RESULTS

Having assembled the logic and mathematical relation-
ships with the empirically tuned flow correction factors,
the model can be used to provide information about the sin-
gle screw compressor. In Figure 35, discharge pressure
versus volumetric efficiency is plotted. The curve is a
least squares fit of the empirical data corrected to an
inlet air temperature of 24 C. The points were evaluated by
the computer model at the same inlet air temperature and
respective discharge pressure.

In Figure 36, inlet air temperature versus volumetric
efficiency is plotted. This is evaluated at a discharge
pressure of 965 KPa. The curve is a least squares fit of
the empirical data and the points were evaluated by the com-
puter model at the same discharge pressure and respective
inlet air temperature.

In Figures 37 and 38, discharge pressure versus
volumetric efficiency is plotted. Figure 37 is the star
rotor tip clearance and Figure 38 is the star rotor window
clearance. The curves on both figures are least squares
fits of the empirical data for the denoted clearance and the
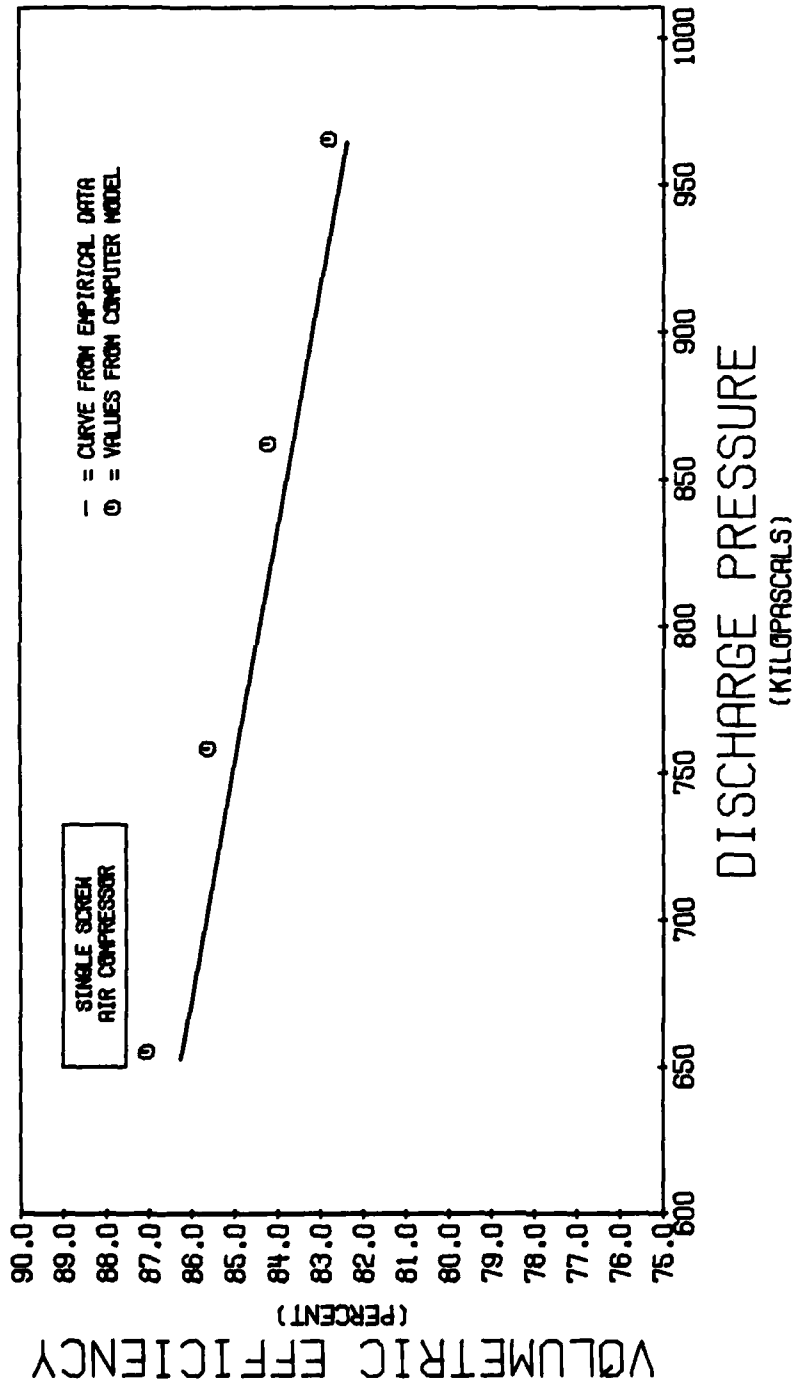points were evaluated by the computer model. The empirical

Figure 35.
Volumetric Efficiency as a Function of
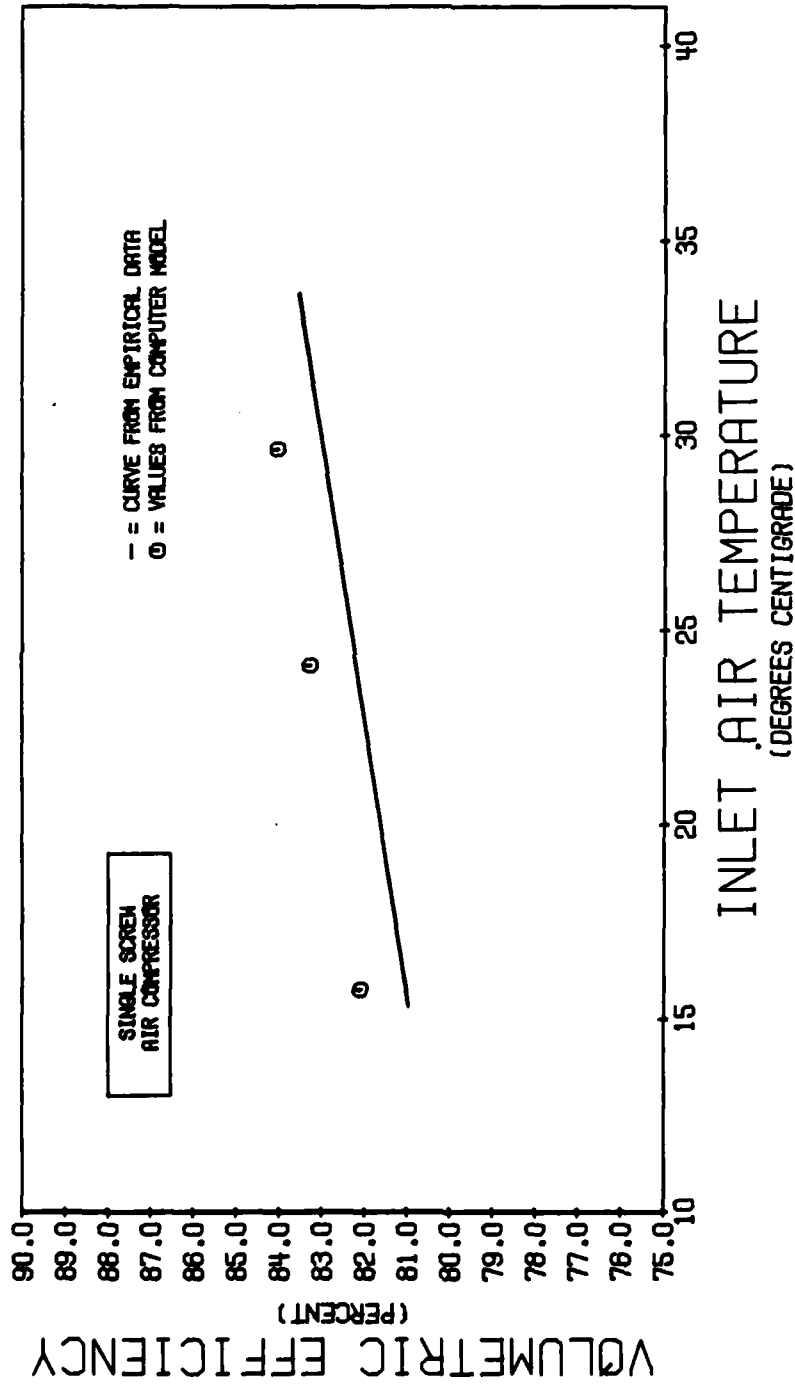Discharge Pressure - Model Values

Figure 36.
Volumetric Efficiency as a Function of Inlet
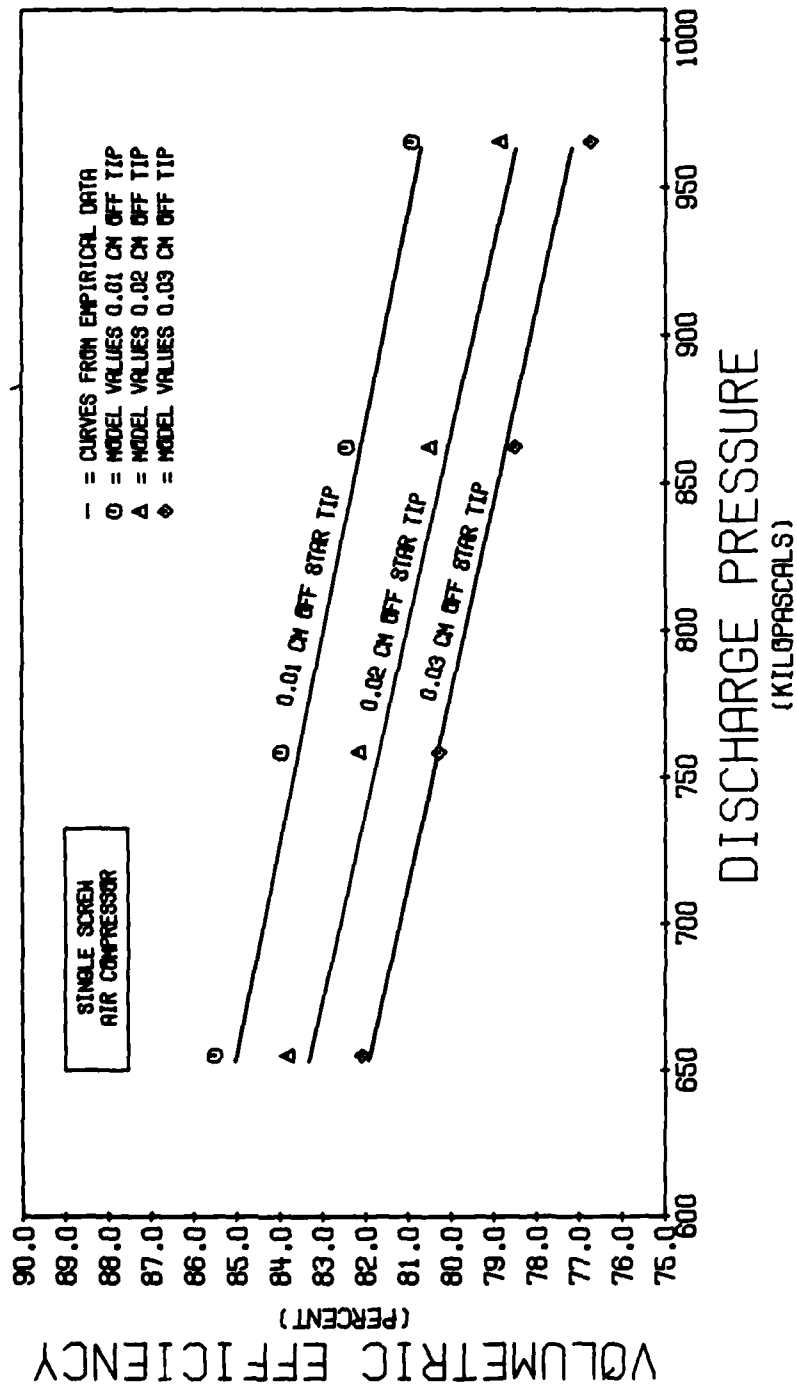Air Temperature - Model Values

Figure 37.
Volumetric Efficiency for Changes in Star
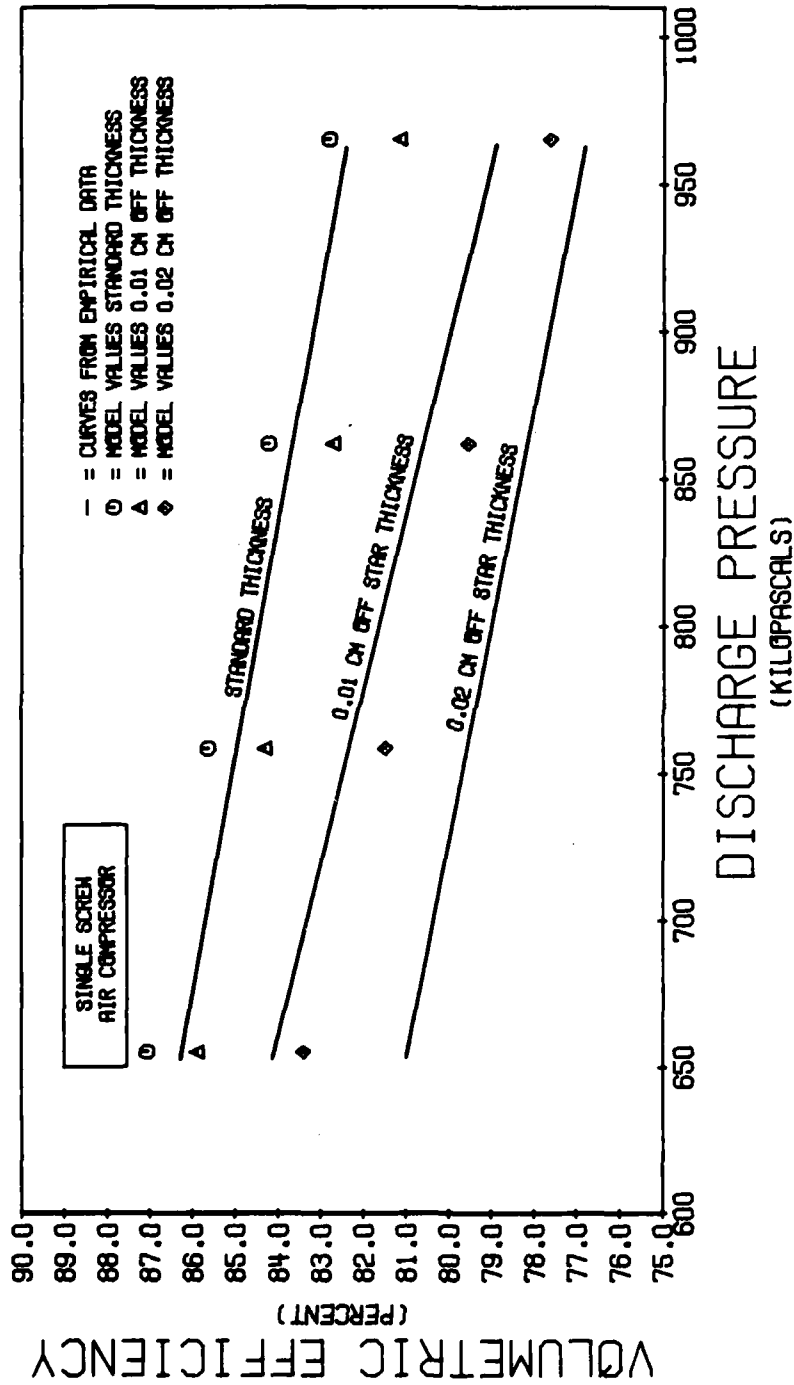Tip Clearance - Model Values

Figure 38.
Volumetric Efficiency as a Function of
Star Window Clearance

data was corrected to an inlet air temperature of 24 C. The
model values were computed at the same inlet air temperature
with the corresponding clearance.

Examining Figure 35, the predicted values of volumetric
efficiency compare very well with the empirical data. This
result is not surprising at the point where the correction
factors were evaluated, 965 KPa discharge pressure. The
close proximity of the predicted values at other than 965
KPa discharge pressure is also encouraging.

However, these predicted values should be regarded
skeptically for the moment, because the sensitivity of the
model to the correction factor for the discharge port leak-
age path.   The predicted values in Figure 35 could all be
produced by an appropriate choice of the correction factor
for the discharge port, with all of the other leakage paths
closed. But, if the empirical curve in Figure 35 is
extended back to a discharge pressure of 101 KPa, the effect
on volumetric efficiency due to the discharge port leakage
path can be eliminated. This extrapolation of Figure 35 is
shown in Figure 39. Also plotted, is the predicted value
for a discharge pressure of 101 KPa. At this point, the
contributor to the volumetric efficiency that is very sensi-
tive to the choice of correction factor is eliminated and
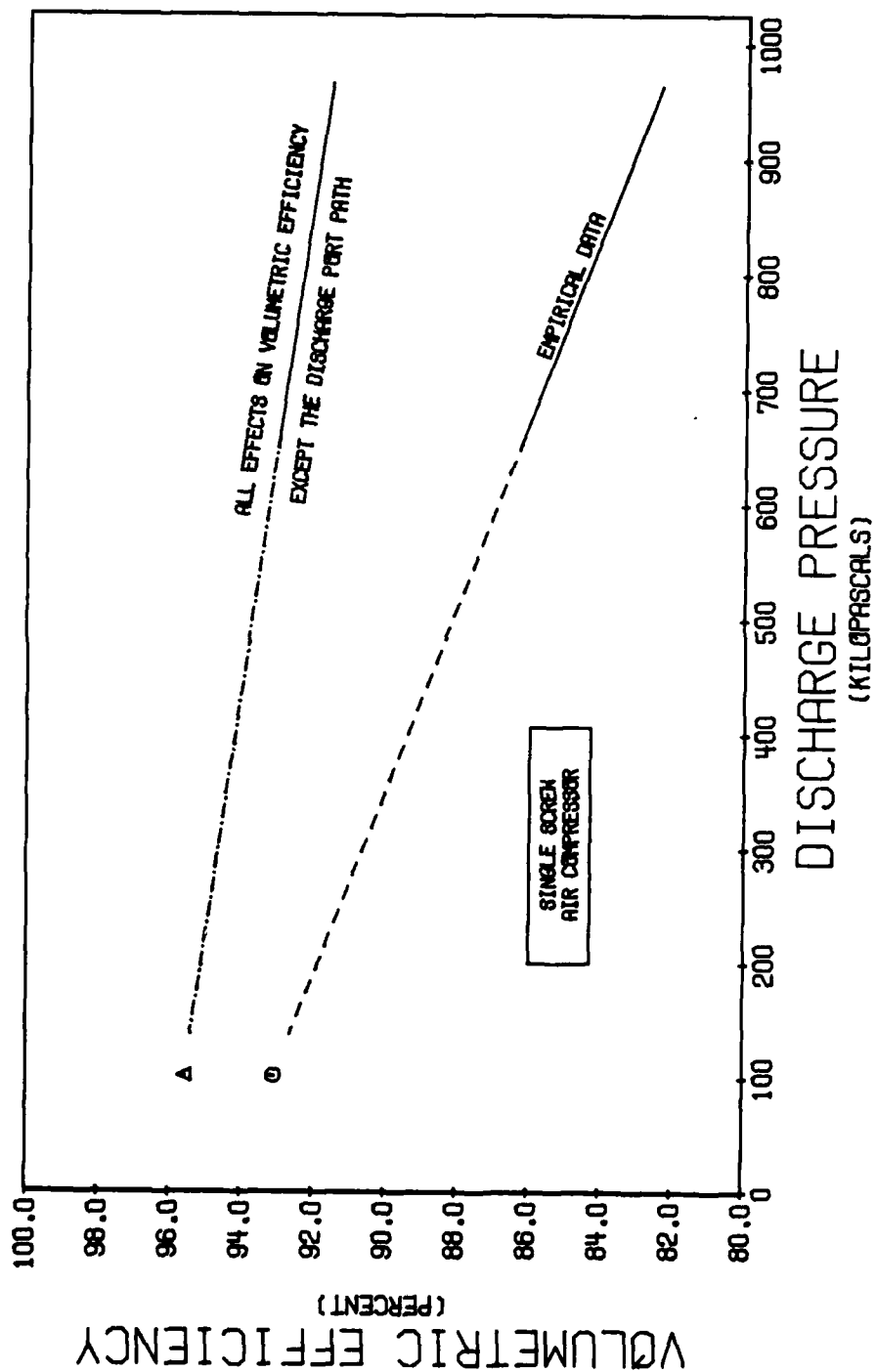the predicted value is with 2.5 % of the extrapolated empir-
ical value.

Figure 39.
Volumetric Efficiency as a Function of
Discharge Pressure - Extrapolated

Figure 40, is a continuation of the idea of separating the volumetric efficiency loss due to the discharge port leakage path from all of the other effects.

In Figure 40, the contribution to the volume efficiency versus the discharge pressure is plotted. As expected, the loss through the discharge port leakage path starts at zero, when the discharge pressure equals suction pressure. The contribution by the combination of the other effects does not start at zero, when the discharge pressure equals suction pressure. This is also shown in Figure 39, and is a result of the built-in volume ratio. The discharge pressure does influence the loss due to the combination of the other effects. However, even when the discharge pressure equals the suction pressure, the pressure in the control volume during the closed compression process is still a function of the built-in volume ratio, the amount of heat transferred during compression, and the leakage in or out of the control volume.

The predicted pressure history through the entire compression cycle is shown in Figure 41. The values are the pressure within the control volume after the model has stabilized and has reached a steady state. The pressure is plotted versus main rotor angle with marks to indicate where the closed compression process begins and where the discharge port opens. Figure 42 is the predicted temperature history versus main rotor angle.
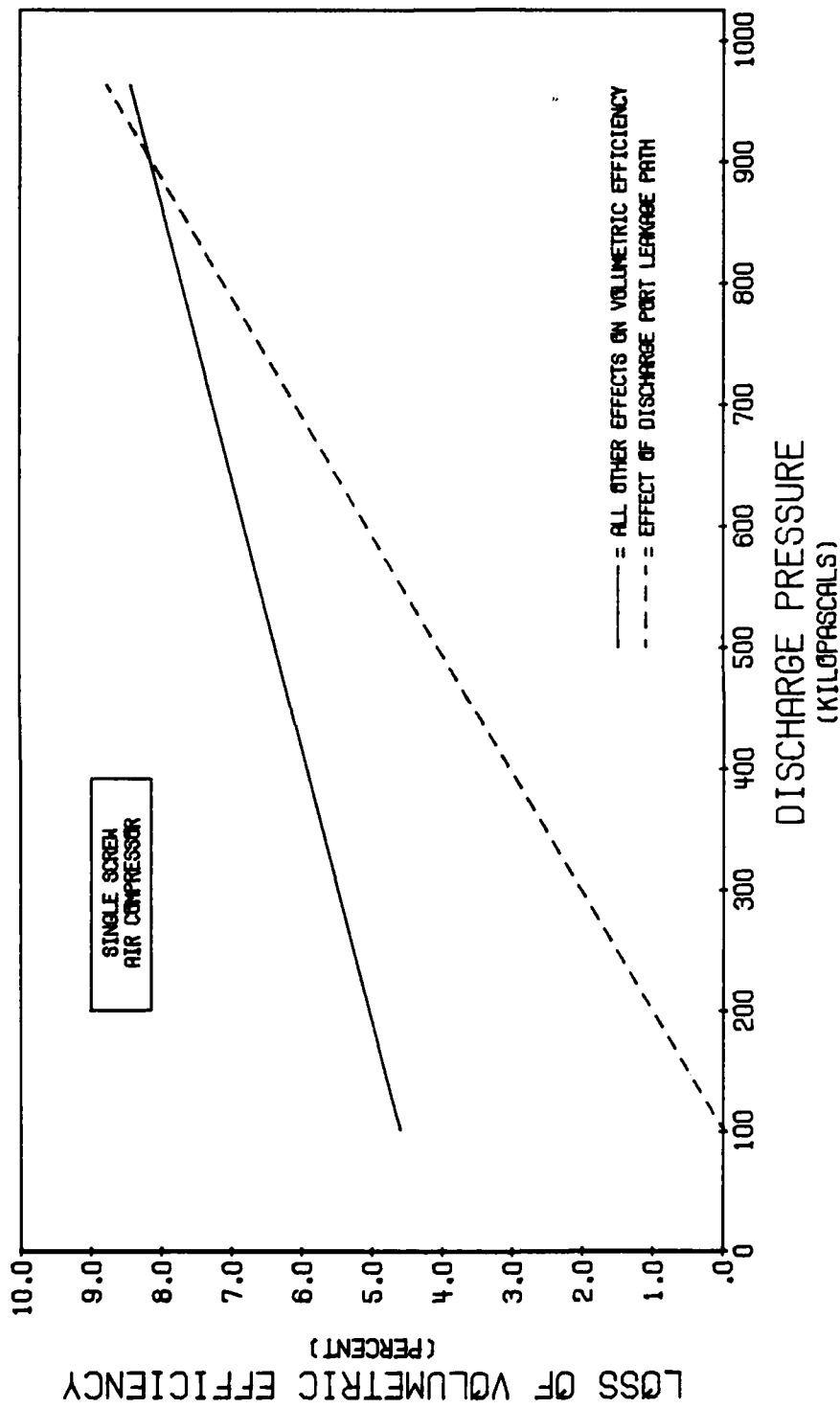
Figure 40.
Loss in Volumetric Efficiency as a Function
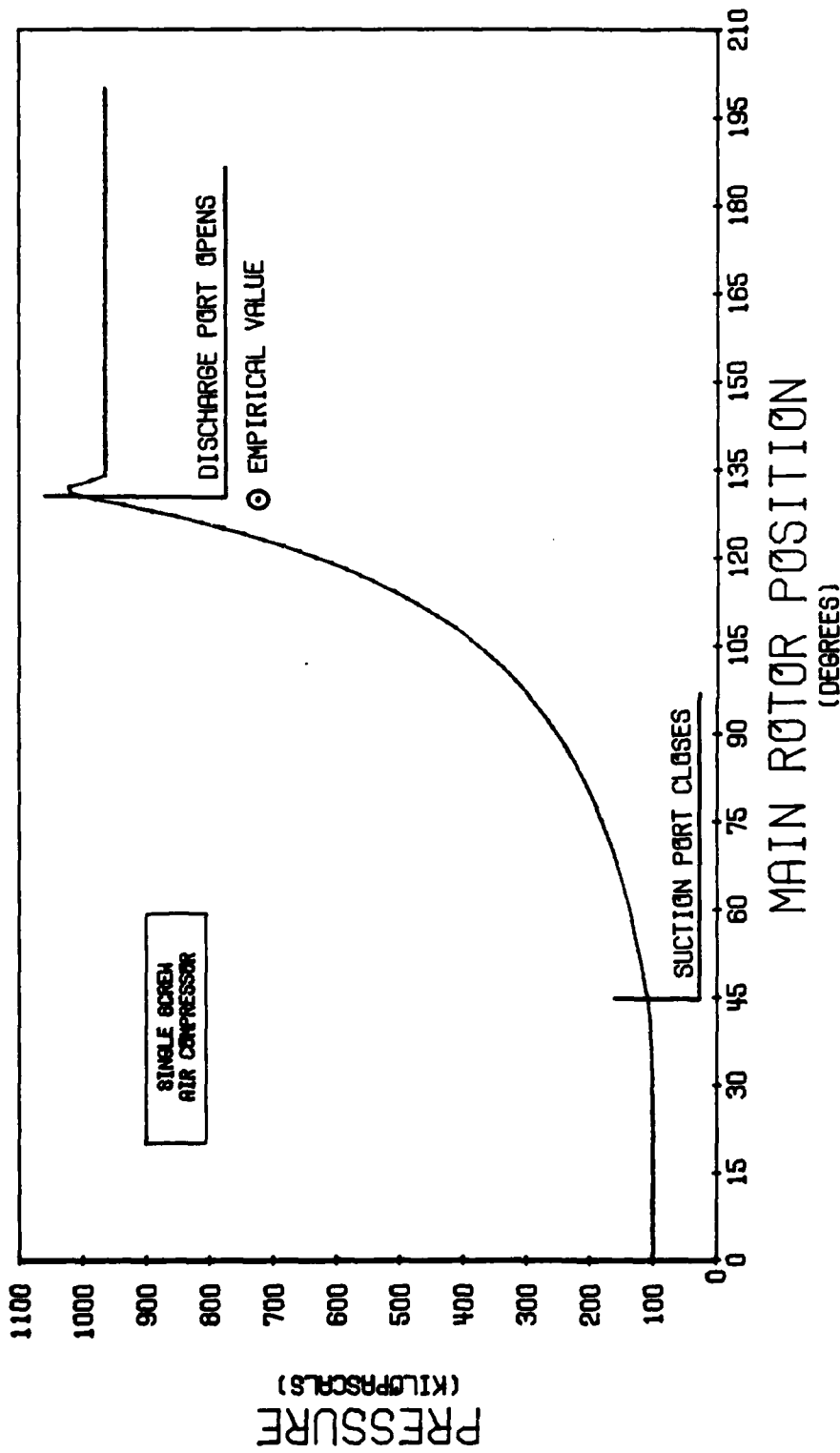of Discharge Pressure

Figure 41.
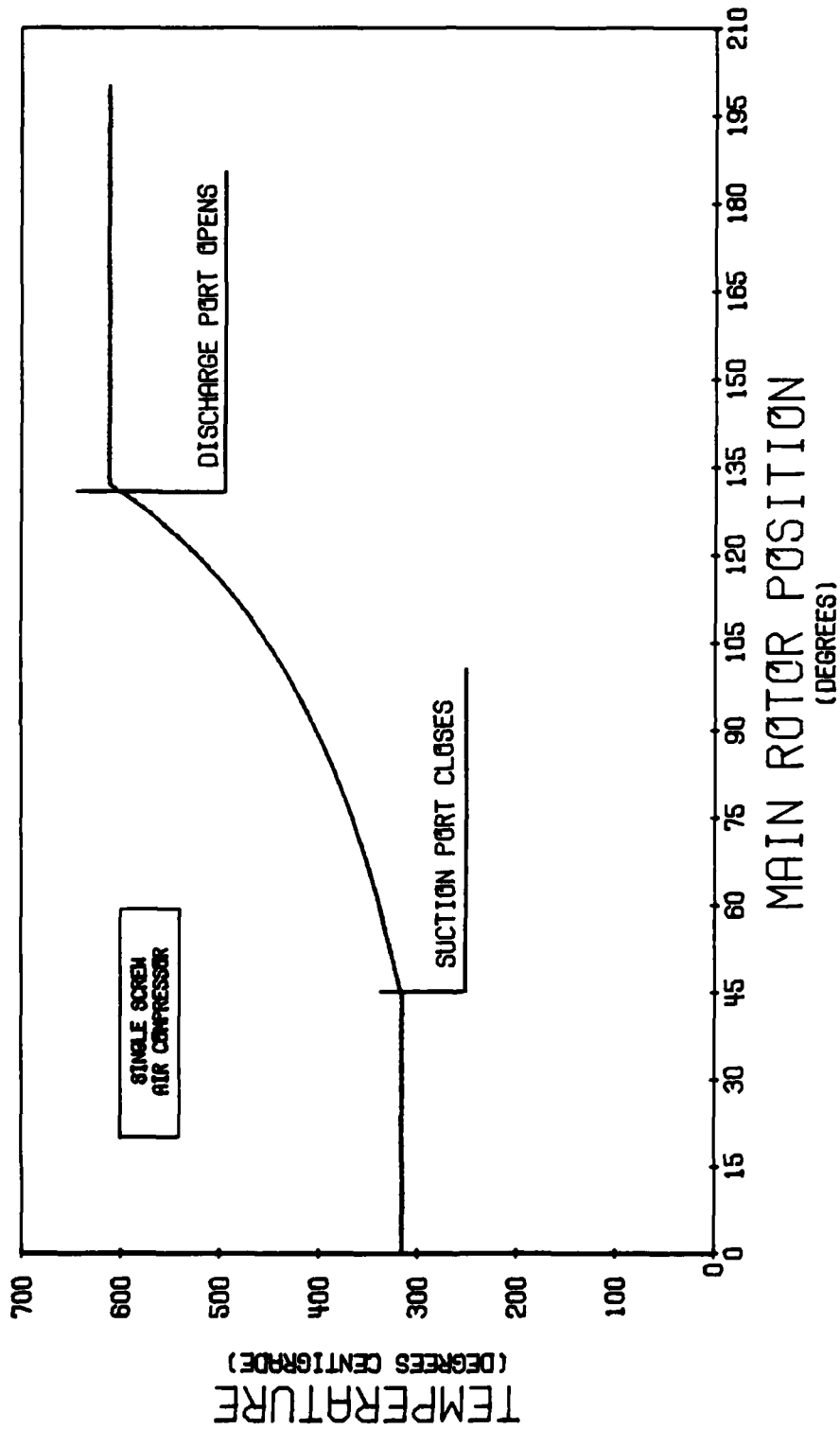Pressure History During Compression Process

Figure 42.
Temperature History During Compression Process

Measurements of the pressure in a thread of an operating compressor are not available. However, tests were made that determined the approximate pressure, 723 KPa, in the thread, when the discharge port opened. To compare this value to the model prediction, this point is also shown on Figure 41. The predicted pressure is 25% lower than the empirically determined value.

It is recognized that, comparing one point in the pressure history does not establish a sufficient basis to assess the accuracy of the model. But it should be noted, that the model does not employ correction factors on the pressure within the control volume. The pressure within the control volume is a function of the heat transferred during the cycle, the geometric relationships, and the type and amount of leakage from the control volume.

The value of the polytropic exponent that the model evaluated in order to try to meet the air-oil bulk discharge temperature was 1.4. The predicted bulk air-oil discharge temperature was 62 C. , whereas the empirical value was 65 C. The model was limited to a maximum polytropic exponent of 1.4 and the lower air-oil bulk discharge temperature indicates that heat is transferred into the control volume. This heat gain is most likely a result of an assumption in the model that the oil that leaks between control volumes stays at the oil injection temperature. The oil will increase in temperature just by friction, which would be

enough to allow the predicted bulk temperature to reach the empirical bulk temperature.

Figure 43 is a plot of the contributions to the volumetric efficiency from each of the effects discussed and for each of the leakage paths evaluated at a discharge pressure of 965 KPa. The main rotor leading land leakage path communicates directly with control volume I only before suction closure. There continues to be leakage across the leading land after suction closure, but the fluid is going into control volume II. Although fluid leaking past the leading land does not go directly into control volume I, and thereby, reducing the available volume for air, it does effect the pressure within the control volume, thereby effecting the leakage through the other paths. The values plotted are the contributions from each of the effects and leakage paths evaluated when the leading land leakage path was closed after suction closure. The leading land leakage was opened and the model was run again. The difference between the total volumetric efficiencies for the open and closed leading land leakage, plus the amount of leakage that goes directly into control volume I, before suction closure, is the value plotted as the contribution to the volumetric efficiency due to the leading land leakage path. Figure 43 is useful as a design tool, to establish where the most significant improvements can be made in the performance of the compressor.
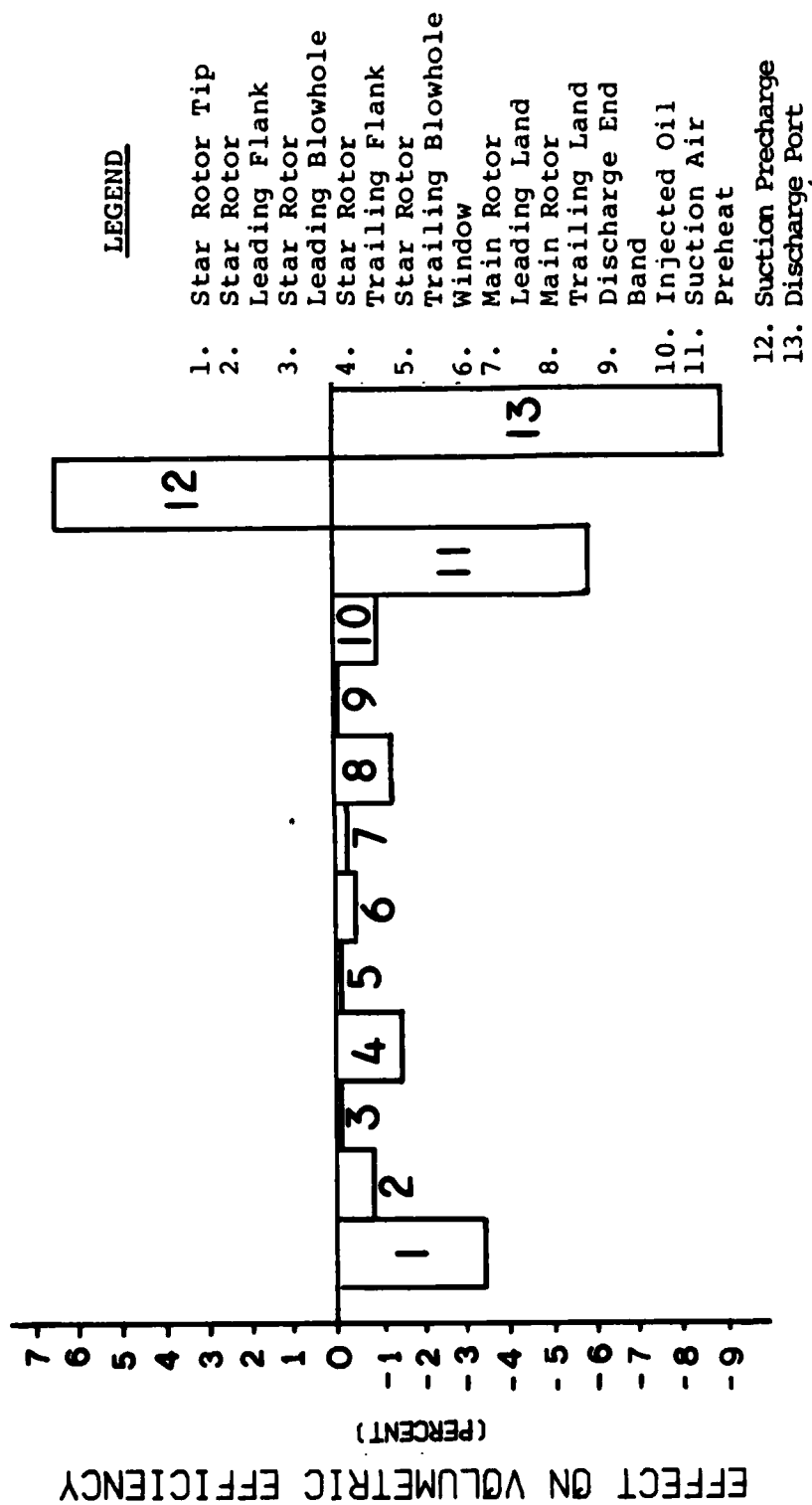
LEGEND

1. Star Rotor Tip
2. Star Rotor
   Leading Flank
3. Star Rotor
   Leading Blowhole
4. Star Rotor
   Trailing Flank
5. Star Rotor
   Trailing Blowhole
6. Window
7. Main Rotor
   Leading Land
8. Main Rotor
   Trailing Land
9. Discharge End
   Band
10. Injected Oil
11. Suction Air
    Preheat
12. Suction Precharge
13. Discharge Port

Figure 43.
Effect of Individual Leakage Paths on the
Volumetric Efficiency

CONCLUSIONS

From the results of the comparison between the computer model and the empirical data, the following conclusions can be drawn:

1. A computer model can be constructed to predict the internal performance of a single screw compressor by adjusting correction factors in the model to produce empirical external data.

2. The fluid that passes through the leakage paths in the boundary of the control volume can be modeled as being only oil, if a correction is applied to the non-viscous effects.

3. The viscous losses for oil flow through non-parallel wall leakage paths can be approximated by integrating Darcy's equation.

4. The closed compression process can be modeled as an isentropic process.

5. There is insignificant heat transfer between the air and oil during the compression process. The majority of the heat transfer between the air and oil occurs in the discharge port.

RECOMMENDATIONS

The amount of oil injection for optimum compressor performance is an area that requires additional effort. The amount of oil injected into the control volume for this task was known to be the optimum based on empirical evaluation. The model assumed that there was always enough oil present at the leakage sites to prevent air from leaking. The ability to predict the performance of the compressor for different oil injection rates would be a substantial addition to the model.

Additional tests should be performed to determine the actual pressure history in the operating compressor. This could then be compared to the predicted pressure from the model. The apparent conclusions from this task would then be either supported or disputed. The assumption that there is insignificant heat transfer between the air and oil in the control volume would also be re-evaluated.

In order to become a truly useful tool for designing single screw compressors, the computer model developed for this task must be modified. The dependency of the model on empirical values must be eliminated. To be useful for the evaluation of various design configurations, the following

variables should be necessary input parameters:

1.   Primary independent variables

   a)   NM   = Number of threads in main rotor.

   b)   NS   = Number of star teeth.

   c)   NSTARS = Number of star rotors.

   d)   RI   = Star rotor inner radius.

   e)   RM   = Main rotor radius.

   f)   RS   = Star rotor outer radius.

   g)   w   = Width of star tooth.

2.   Secondary variables:

   a) θ_{STSC} = Star tooth centerline angle at suction
        closure.

   b) θ_{MRINJ} = Main rotor angle, relative to suction
        closure, where oil injection begins.

   c)   DVRATIO = Ratio of volume in thread before suction
        closure to volume in thread when discharge begins.

3.   System values:

   a)   Inlet pressure and temperature.

   b)   Discharge pressure.

   c)   Oil injection temperature.

d)   Main rotor speed.

4.   Functions to generate property values of air.

5.   Functions to generate property values of oil.

Relationships will need to be developed to replace the empirical values presently used.

The correction factors on the non-viscous losses would need to be eliminated.   It may be possible to develope a relationship to determine the correction factor from the poiseuille flow velocity and the speed the wall moves relative to the leakage site. Tests should also be conducted, on a basic level, to evaluate the flow through the types of leakage paths encountered in the single screw compressor under controlled conditions. These tests would be useful to develop a better understanding of the processes and effects of this type of flow. The tests would also serve as a basis for comparison of the conclusions drawn from this task.

Relationships would also need to be developed for the discharge port correction factor. The factors that would appear to be necessary to develop a relationship are; the discharge pressure, the oil viscosity, the size of the discharge port, the main rotor speed, and, the relation of open thread area to land area on the main rotor. Conducting tests on the compressor at various speeds, and, if possible, different oil viscosities, would provide insight into the

problem. Even if a direct, functional-type relationship could not be identified, a range for the correction factor would be determined by the empirical data.

While evaluating various designs, the clearances should be set internally by the model. This could be done by using typical values from a known geometry and using size ratios, based on the primary independent variables, to set clearances for a different geometry. In this way, the designs would be judged from a common basis. However, when a particular design is chosen for further evaluation, the model should allow the clearances to be input as variables. This would allow evaluation of the sensitivity of a particular design to necessary manufacturing tolerances.

The conclusion that the closed compression process is isentropic, simplifies the thermodynamic portion of the model and eliminates the need for an empirical value for the bulk air-oil temperature. The ratio of specific heats can be used in place of the polytropic exponent. The bulk air-oil discharge temperature can then be predicted by the calculated conditions in the control volume, when the discharge port opens. The tests to determine the actual pressure history may alter the isentropic compression conclusion, but, it still should be possible to establish the process with a fixed polytropic exponent.

The correct amount of oil to be injected into the

control volume is another area where changes will be needed. Techniques need to be developed, so that a criteria can be established to evaluate the optimum amount of oil injection for arbitrary geometries. When this criteria is available, it will be possible to take the empirical data associated with oil injection, out of the model.

REFERENCES

1. Wojciechowski,Felix, <u>Machine Design</u> ,Jan 22,1976,p105.

2. Beyer,William H., <u>CRC Standard Mathematical Tables</u> ,25th edition,1978,CRC Press,Florida,p150.

3. Hseigh,Jui S., <u>Principles of Thermodynamics</u> ,1975,Scripta,Washington,D.C.

4. Fox,R.W. and McDonald,A.T., <u>Introdction to Fluid Mechanics</u> ,2nd edition,1978,John Wiley,New York.

5. The Engineering Division, <u>Flow of Fluids Through Valves, Fittings, and Pipe</u> ,Technical Paper 410,1979,The Crane Company,NewYork.

6. Stepanoff,A.J., <u>Centrifugal and Axial Flow Pumps</u> ,1948,John Wiley,New York.

7. Soedel,Werner, <u>Introduction to Computer Simulation of Positive Displacement Compressors</u> ,Ray W. Herrick Laboratories,Purdue University,July 1972.

DISTRIBUTION

NAVSEA

2 SEA 05R1

2 SEA 5321/J. ISOLATO

2 SEA 996

12 DTIC

CENTER DISTRIBUTION

COPIES	CODE	NAME
1	2702	W. Levedahl
1	272	E. Quandt
2	2722	J. Ward
5	2722	H. Skruch
15	2722	T. Bein
1	2722S	
1	522.1	Unclassified Library (C)
1	522.2	Unclassified Library (A)
2	5231	Office Services